DNA Repair 10 (2011) 314–321

Contents lists available at ScienceDirect

DNA Repair

journal homepage: www.elsevier.com/locate/dnarepair

Two unrelated patients with *MRE11A* mutations and Nijmegen breakage syndrome-like severe microcephaly

Yoshiyuki Matsumoto[a], Tatsuo Miyamoto[a], Hiromi Sakamoto[a], Hideki Izumi[a], Yuka Nakazawa[b], Tomoo Ogi[b], Hidetoshi Tahara[c], Shozo Oku[d], Azuma Hiramoto[e], Toshihide Shiiki[f], Yoshiki Fujisawa[g], Hirofumi Ohashi[h], Yoshihiro Sakemi[i], Shinya Matsuura[a,*]

[a] *Department of Genetics and Cell Biology, Research Institute for Radiation Biology and Medicine, Hiroshima University, Kasumi 1-2-3, Minami-ku, Hiroshima 734-8553, Japan*
[b] *Department of Molecular Medicine, Atomic Bomb Disease Institute, Nagasaki University, Sakamoto 1-12-4, Nagasaki 852-8523, Japan*
[c] *Department of Cellular and Molecular Biology, Graduate School of Biomedical Sciences, Hiroshima University, Kasumi 1-2-3, Minami-ku, Hiroshima 734-8553, Japan*
[d] *Kagoshima Kodomo Hospital, Ijuin-cho 2-2000-669, Hioki 899-2503, Japan*
[e] *Hokkaido Ryoikuen, Shunkoudai 4-10, Asahikawa 071-8144, Japan*
[f] *Tobu Ryoiku Center, Shinsuna 3-3-25, Koutou-ku 136-0075, Tokyo, Japan*
[g] *Ehime Prefectural Central Hospital, Kasugamachi 83, Matsuyama 790-0024, Japan*
[h] *Saitama Children's Medical Center, Iwatsuki-ku, Saitama 339-8551, Japan*
[i] *Beppu Medical Center, Uchikamado, Beppu 874-0011, Japan*

ARTICLE INFO

Article history:
Received 19 August 2010
Received in revised form
25 November 2010
Accepted 10 December 2010
Available online 12 January 2011

Keywords:
Nijmegen breakage syndrome (NBS)
Ataxia–telangiectasia-like disorder (ATLD)
Nijmegen breakage syndrome-like disorder (NBSLD)
ATM
MRE11
NBS1
Microcephaly

ABSTRACT

MRE11 and NBS1 function together as components of a MRE11/RAD50/NBS1 protein complex, however deficiency of either protein does not result in the same clinical features. Mutations in the *NBN* gene underlie Nijmegen breakage syndrome (NBS), a chromosomal instability syndrome characterized by microcephaly, bird-like faces, growth and mental retardation, and cellular radiosensitivity. Additionally, mutations in the *MRE11A* gene are known to lead to an ataxia–telangiectasia-like disorder (ATLD), a late-onset, slowly progressive variant of ataxia–telangiectasia without microcephaly. Here we describe two unrelated patients with NBS-like severe microcephaly (head circumference −10.2 SD and −12.8 SD) and mutations in the *MRE11A* gene. Both patients were compound heterozygotes for a truncating or missense mutation and carried a translationally silent mutation. The truncating and missense mutations were assumed to be functionally debilitating. The translationally silent mutation common to both patients had an effect on splicing efficiency resulting in reduced but normal MRE11 protein. Their levels of radiation-induced activation of ATM were higher than those in ATLD cells.

1. Introduction

The development of the central nervous system is highly sensitive to DNA damaging agents and therefore several autosomal recessive disorders with defective DNA damage repair exhibit neurological abnormalities such as microcephaly and neurodegeneration [1,2].

The MRE11/RAD50/NBS1 (MRN) protein complex and the ataxia–telangiectasia mutated (ATM) protein, together play a central role in DNA double strand break repair [3]. Mutations in the *ATM* (MIM# 607585) and *MRE11A* (MIM# 600814) genes each give rise to a progressive cerebellar ataxia syndrome: *ATM* mutations to ataxia–telangiectasia (A–T [MIM# 208900]) [4], and *MRE11A* mutations to ataxia–telangiectasia-like disorder (ATLD [MIM# 604391]) [5,6]. A–T is an autosomal recessive disorder characterized by growth deficiency, progressive cerebellar ataxia, dysarthria, telangiectasia, frequent respiratory infections, and immunodeficiency. ATLD is also characterized by cerebellar ataxia, but its onset is later in life and its progression is slower than in A–T. In addition, there is no telangiectasia and immunoglobulin levels are normal.

Mutations in two different genes involved in the MRE11/RAD50/NBS1 complex are known to lead to a hereditary disorder with severe microcephaly: the *NBN* gene (MIM# 602667) to Nijmegen breakage syndrome (NBS [MIM# 251260]) [7–9], and the *RAD50* gene (MIM# 604040) to Nijmegen breakage syndrome-like disorder (NBSLD [MIM# 613078]) [10]. NBS is an autosomal recessive disorder characterized by microcephaly, growth and mental retardation, immunodeficiency, radiosensitivity, and cancer predisposition; NBSLD is a disorder with microcephaly, mental retardation, bird-like face, and short stature,

* Corresponding author. Tel.: +81 82 257 5809; fax: +81 82 256 7101.
E-mail address: shinya@hiroshima-u.ac.jp (S. Matsuura).

1568-7864/$ – see front matter © 2010 Elsevier B.V. All rights reserved.
doi:10.1016/j.dnarep.2010.12.002

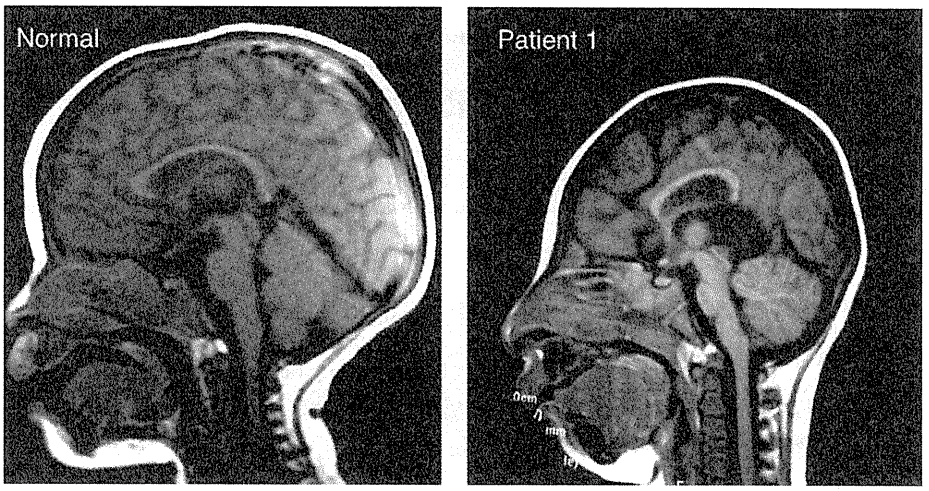

Fig. 1. Sagittal brain magnetic resonance imaging. (Left) Normal individual. (Right) Patient 1 at age 18 months with generalized cerebral hypodysplasia.

but without severe infections, immunodeficiency, or cancer predisposition.

We here describe two unrelated patients with Nijmegen breakage syndrome-like severe microcephaly and compound heterozygous mutations in the *MRE11A* gene.

2. Materials and methods

2.1. Clinical report

A 35-year-old woman was referred to us at 18 weeks of pregnancy for evaluation of intrauterine growth retardation. Ultrasound scan showed a fetus with a small femora and a disproportionately small head. Caesarian section was performed at 32 weeks of pregnancy, and a boy (Patient 1), was delivered. His birth weight was 966 g (−4.8 SD), length 35 cm (−6.7 SD), and head circumference 22 cm (−8.1 SD). He had severe microcephaly, a bird-headed facial appearance with receding forehead, and a prominent nose. Anterior fontanel was not palpable. His parents and two elder brothers were all healthy and phenotypically normal. There was no family history of consanguinity. Brain magnetic resonance imaging at age 18 months demonstrated hypoplasia of the cerebrum, smooth gyri, and enlarged lateral ventricles (Fig. 1). He had patent ductus arteriosus, which was surgically corrected at age 5 months. Bilateral cryptochidism was operated on at age 3 years. He stood holding onto a chair at age 30 months, sat alone with a stoop at age 3 years, and walked at age 3 years. At age 3.5 years, he weighed 7.4 kg (−4.1 SD), measured 78.5 cm (−4.8 SD), and had a head circumference of 34 cm (−10.2 SD). G-banded chromosomes were 46, XY. He had no severe or recurrent infections and his immunoglobulin levels were normal. Now aged 8 years, he is toilet trained, speaks several meaningful words, but does not speak a two-word-sentence. He attends a primary school, and is affable and friendly. He is farsighted with astigmatism. He is able to run with a slow pitch and kick a soccer ball. He shows neither ocular apraxia nor cerebellar ataxia.

Patient 2, a boy, was born at 37 weeks of gestation to a 29-year-old mother and a 28-year-old father, both healthy and unrelated. The pregnancy was unremarkable. An older brother was healthy without malformations. Birth weight was 1560 g (−4.1 SD), length 39 cm (−5.9 SD), and head circumference 25 cm (−6.1 SD). At age 30 months, he sat alone but could not stand or walk. At age 5 years, he shuffled while sitting, but was unable to stand. At age 13 years, he weighed 9.2 kg (−4.2 SD), measured 97 cm (−7.0 SD), and had a head circumference of 35 cm (−12.8 SD). He had severe microcephaly, a bird-like face with sloping forehead, a big nose, large and simple ears, short palpebral fissures, a small mouth, and a small and receding chin. His shoulders, elbows, hips, and knees exhibited a decreased range of motion. Also noted were scoliosis, subluxation of the left elbow joint, bilateral cryptorchidism, and bilateral talipes equinus. His tendon reflexes were slightly exaggerated. G-banded chromosomes were 46, XY. His immunoglobulin levels were normal. Now aged 33, he lives in an institution for handicapped individuals. He does not speak meaningful words, but recognizes people, communicates by gesture, and shows fondness by touching. He is bedridden, is unable to roll over, and is handfed. He did not develop secondary sexual characteristics. He does not show ocular apraxia and had neither malignancy nor severe infections.

2.2. Immortalized skin fibroblast cells

Informed consent was obtained from Patients 1 and 2 and their families prior to this study. Primary skin fibroblast cells cultured from the two patients were immortalized by transfection with an SV40 virus and phTERT retrovirus vector [11]. We used as references immortalized fibroblast cell lines (designated as SVT) from various related disorders: NBS (GM7166VA7) [12], A–T (AT5BIVA) [13], and ATLD (D6807-SVT) [6,14]. A fibroblast cell line from a normal individual (SM-SVT) served as a control. A mouse hybrid cell line A9(neo11)-1 containing human chromosome 11 was provided by Dr. M. Oshimura, and microcell-mediated chromosome transfer was performed as previously described [12]. Fibroblast cell lines were maintained in D-MEM supplemented with 10% fetal bovine serum (Hyclone, Logan, UT, USA).

2.3. EB virus-transformed lymphoblastoid cell lines (LCLs)

LCLs were established from peripheral blood lymphocytes of the two patients and their family members. We used LCLs from NBS (94P247) [9], ATLD (200704L), and A–T as references, and a LCL from a normal individual (96-007M) as a control. A NBS cell line (94P247) was provided by Dr. K. Sperling. An ATLD cell line (200704L) was established from a blood sample from a boy with ATLD [15], supplied by Drs. S. Nonoyama and K. Imai. LCLs were cultured in RPMI 1640 with 20% fetal bovine serum.

2.4. Mutational analysis

PCR primers for *MRE11A* gene (GenBank NM_005591.3) were synthesized to amplify all coding exons and intron–exon boundaries [16]. PCR products were directly sequenced using an ABI

PRISM 3130 Genetic Analyzer (Applied Biosystems, Foster City, CA). RT-PCR primers were synthesized to amplify the *MRE11A* cDNA spanning exons 1–8 (5′-CGAAAAGAAGACAGCCTTGG-3′ and 5′-TCCAAAAATTGTTCTGGAATGA-3′) (GenBank NM_005590.3). RT-PCR products were visualized following electrophoresis on a 2% NuSieve agarose gel. PCR primers for *RAD50* (GenBank Z75311.1) and *NBN* cDNAs (GenBank AF058696.2) were synthesized to amplify the open reading frame with several overlapping segments.

Transcript levels of the *MRE11A*-c.338A and *MRE11A*-c.338G alleles in LCLs from a normal individual, Patient 2 and the parents were determined by the cycleave quantitative real time PCR assay (Cycleave-qPCR, TaKaRa Co. Ltd.) carried out in triplicate. Transcripts from the *HPRT1* allele were used as a quantification control. RNaseH sensitive fluorescent probes that specifically recognize the *MRE11A*-c.338A and *MRE11A*-c.338G alleles were used for the assay. The qPCR results were analyzed by the ΔΔCT method. qPCR primers and probes used for the assay are listed below.

MRE11A-F: 5′-ACGTTTGTAACACTCGATGAA-3′;
MRE11A-R: 5′-CTGGAATTGAAATGTTGAGG-3′;
MRE11Ac.338A: (Eclipse) 5′-dAdAdG(A)dTdGdGdCdAdA-3′ (FAM);
MRE11Ac.338G: (Eclipse) 5′-dAdAdG(G)dTdGdGdCdA-3′ (ROX);
HPRT1-F: 5′-CAGGCAGTATAATCCAAAGATG-3′;
HPRT1-R: 5′-ACTGGCGATGTCAATAGGA-3′;
HPRT1-probe: (Eclipse) 5′-dCdAdGdCdA(A)dGdCdT-3′ (FAM).

2.5. Western blot analysis

Western blotting was performed as described previously [17]. Primary antibodies used were: mouse anti-MRE11 monoclonal antibody (MRE11-12D7, 1:1000, GeneTex, Irvine, CA); mouse anti-RAD50 monoclonal antibody (13B3/2C6, 1:1000, GeneTex, Irvine, CA); rabbit anti-NBS1 polyclonal antibody (NB100-142, 1:500, Novus Biologicals, Littleton, CO); mouse anti-GAPDH monoclonal antibody (6C5, 1:1000, Santa Cruz Biotechnology, Santa Cruz, CA); and mouse anti-β-tubulin monoclonal antibody (1:2000, Sigma–Aldrich, St. Louis, MO).

2.6. Radiation-sensitivity analysis

Clonogenic analysis was performed on fibroblast cell lines to learn of their radiosensitivity as previously described [12]. Chromosome breakage analysis of LCLs was carried out as follows. Cells were irradiated with 2 Gy X-ray and harvested 24 h after irradiation. Giemsa-stained chromosome slides were prepared, and chromatid or chromosome breaks and quadriradials were counted.

2.7. ATM autophosphorylation after γ-irradiation

Immortalized fibroblast cells or LCLs were irradiated with 0.5 Gy of γ ray. At 15 min and 30 min after irradiation, the cells were analyzed with Western blotting using rabbit anti-ATM-p1981 monoclonal antibody (1:1000, Epitomics Inc., Burlingame, CA) and mouse anti-ATM monoclonal antibody (2C1, 1:1000, GeneTex, Irvine, CA). Band intensities were estimated using a densitometer and are presented as means ± standard deviation. The statistical differences were analyzed with Student's *t*-test. Statistical significance was assumed for $p < 0.05$.

2.8. DNA damage response assay

ATM-dependent G2/M checkpoint arrest was performed according to the methods described previously [18].

2.9. p53 phosphorylation after γ-irradiation

Lymphoblastoid cells were irradiated with 0.5 Gy of γ ray. At 15 min and 30 min after irradiation, the cells were analyzed with Western blotting using rabbit anti-phosphorylated p53 (Ser15) polyclonal antibody (1:1000, Cell Signaling Technology, Beverly, MA) and mouse anti-p53 monoclonal antibody (1:1000, Oncogene Research Products, CA).

2.10. Caspase 3 activation after γ-irradiation

Immortalized fibroblast cells were irradiated with 0 or 10 Gy of γ ray. At 72 h after irradiation the cells were analyzed with Western blotting using rabbit anti-cleaved caspase 3 monoclonal antibody (#9664, 1:1000, Cell Signaling Technology, Beverly, MA).

3. Results

3.1. Identification of MRE11A mutations

Several studies have demonstrated that microcephaly, as was present in the two patients we described, is a common feature in a variety of DNA damage repair defective disorders [2]. Therefore, we examined DNA damage repair proteins including ATM, ATR, MRE11, RAD50, and NBS1 in the two patients. Western blot analysis showed normal levels of ATM and ATR (data not shown) and reduced levels of MRE11, RAD50, and NBS1 in both patients (Fig. 2a). We, therefore, sequenced all the *MRE11A*, *RAD50*, and *NBN* coding sequences in both patients and found only the *MRE11A* mutations c.658A>C and c.659+1G>A in Patient 1, and c.658A>C and c.338A>G in Patient 2 (Fig. 2b). In Patient 1, c.658A>C was derived from the father, and c.659+1G>A from the mother. Two brothers were a heterozygote for c.659+1G>A. RT-PCR and sequencing analysis demonstrated that c.659+1G>A resulted in exon 7 skipping leading to a premature termination codon (p.Ser183ValfsX31) (Fig. 2c). The c.658A>C substitution located within exon 7 did not alter amino acids but affected splicing efficiency that resulted in exon 7 skipping (Fig. 2c). RT-PCR analysis of exons 1–8 of *MRE11A* cDNA from Patient 1 detected a reduced but considerable amount of correctly spliced transcripts in addition to the exon-skipped transcript (Fig. 2c). Western blot analysis of fibroblasts from Patient 1 detected a reduced amount of normal-sized MRE11 protein (Fig. 2a). No smaller-sized protein corresponding to the predicted truncated form was detected in both lymphocytes and fibroblasts. The c.658A>C substitution was not found in 100 normal Japanese individuals. These results indicated that the c.658A>C mutation leads to exon 7 skipping but that some of the RNA is correctly spliced.

Patient 2 was another compound heterozygote with c.658A>C, the same single-base substitution as the one found in Patient 1, and c.338A>G, a single-base substitution in exon 5. The c.658A>C substitution was inherited from the mother while c.338A>G was derived from the father. A DNA sample from the older brother was not available. Cloning and sequencing of the RT-PCR products of Patient 2 revealed two kinds of mRNA from the c.338G allele; normal sized transcripts carrying the c.338A>G substitution and intermediately sized transcripts resulting from exon 5 skipping (Fig. 2c). The normal sized products lead to an amino acid substitution of Asp to Gly at the 113th residue (p.Asp113Gly). The 113th residue is located within the highly conserved phosphoesterase domain, which is essential for endonuclease activity [19]. On the other hand, the intermediately sized transcripts resulting from exon 5 skipping lead to a premature termination codon (p.Phe106GlnfsX10). We then examined the levels of the transcripts from the c.338A and c.338G alleles by quantitative RT-PCR analysis. The correctly spliced

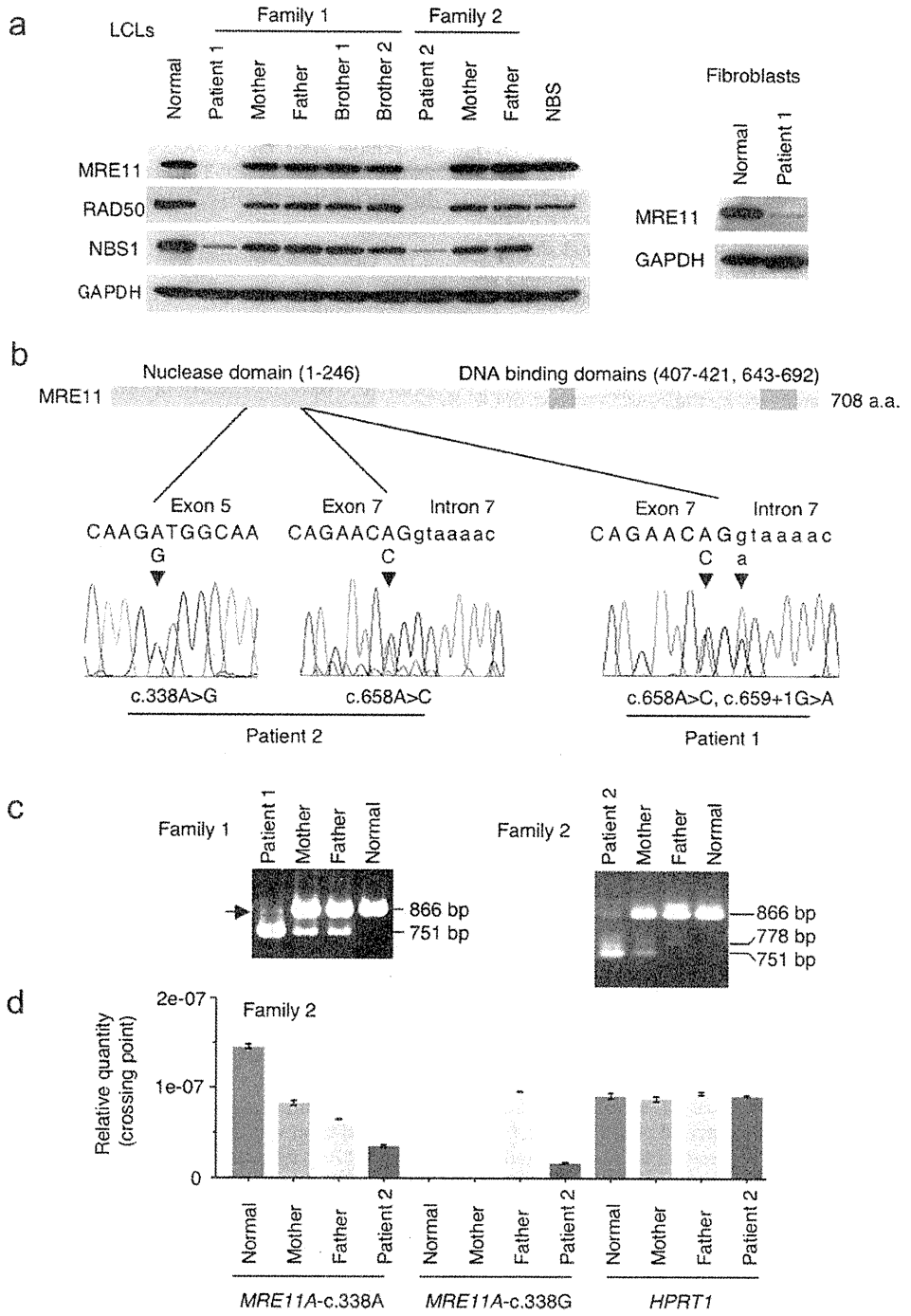

Fig. 2. MRE11 deficiencies associated with *MRE11A* mutations. (a) Western blot analyses of MRE11, RAD50, and NBS1 in lymphoblastoid cell lines (LCLs) from Patients 1 and 2 and their family members. Nijmegen breakage syndrome (NBS) cells were used as an NBS1-deficient reference, and anti-GAPDH antibody for equal loading. Levels of MRE11, RAD50, and NBS1 were reduced in both patients. Right panel shows a reduced MRE11 protein band of normal size in fibroblasts from Patient 1. (b) MRE11 protein structure and *MRE11A* mutations in Patients 1 and 2 as determined by genomic DNA sequencing. Patient 1 was a compound heterozygote with c.658A>C, a single-base substitution in exon 7, and c.659+1G>A, a substitution at an exon–intron junction of the splice donor-site. Patient 2 was a compound heterozygote with c.658A>C, the same single-base substitution in exon 7, and c.338A>G, a single-base substitution in exon 5. (c) RT-PCR analyses of exons 1–8 of *MRE11A* cDNAs from Patients 1 and 2 and their family members. RT-PCR of Patient 1 yielded two bands of 866 bp and 751 bp. The 866 bp band corresponds to the correctly spliced transcripts, and the 751 bp band to exon 7-skipped transcripts. The arrow on the left margin indicates the transcripts from the c.658A>C mutant allele. Analyses in the parents yielded two bands of 866 bp and 751 bp. RT-PCR of Patient 2 showed three bands of 866 bp, 778 bp, and 751 bp. The 866 bp band corresponds to the correctly spliced transcripts from the c.658A>C allele and the c.338A>G allele. The 778 bp band corresponds to exon 5-skipped transcripts, and the 751 bp band to the exon 7-skipped transcripts. (d) Quantitative RT-PCR analysis of the transcript levels from the c.338A and the c.338G alleles of Patient 2 and their family members. Transcripts from the *HPRT1* allele were used as a quantification control. The correctly spliced transcripts from the c.338G allele of Patient 2 showed 25% of the normal level. By contrast, the transcript levels from the c.338G allele of the father were not affected.

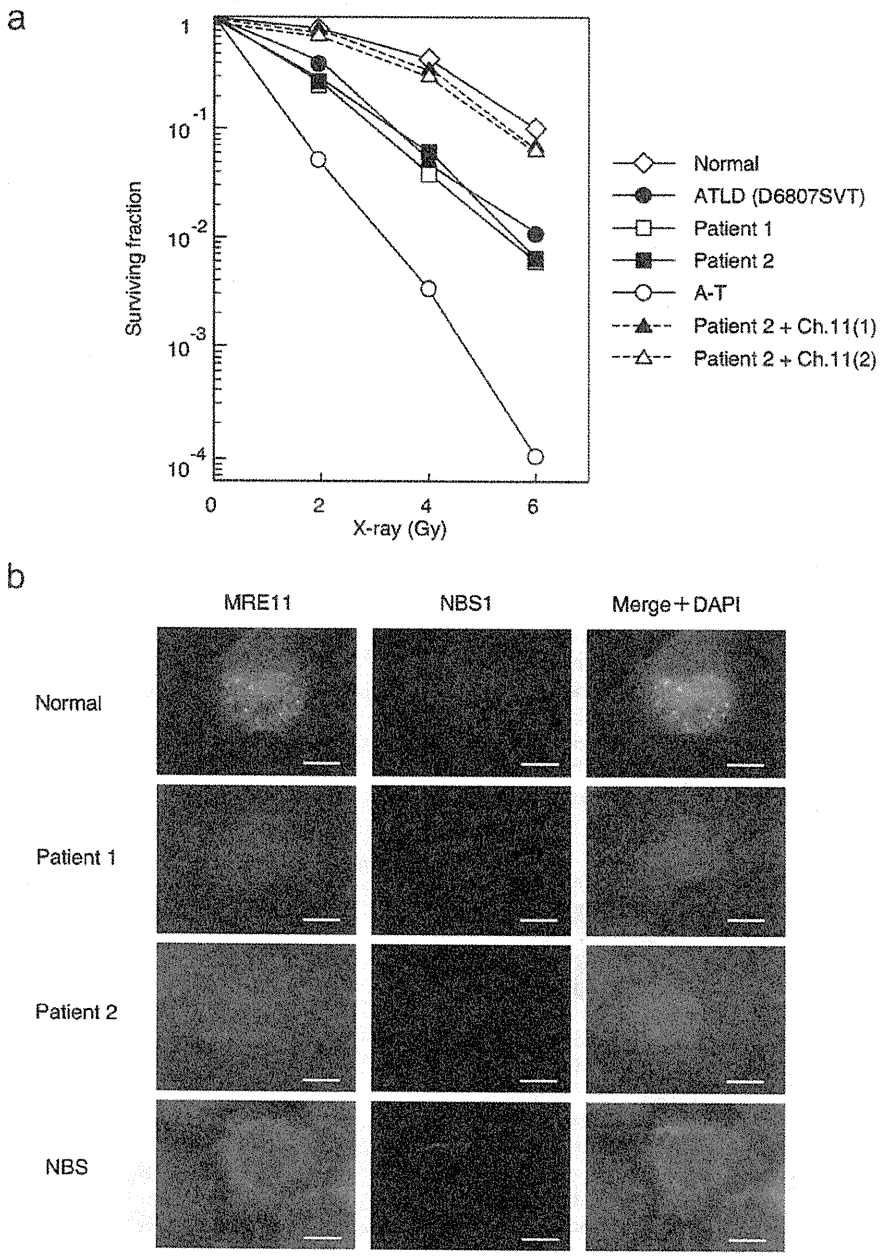

Fig. 3. Clonogenic survival curves for X-ray-irradiated fibroblasts. (a) Radiosensitivity was measured by counting colonies surviving radiation doses of 0–6 Gy. Colony survival was expressed as a logarithm. ATLD, ataxia–telangiectasia-like disorder; A–T, ataxia–telangiectasia. A–T cells were highly sensitive to radiation. Cells from Patients 1 and 2, and ATLD all showed intermediate levels of sensitivity. Microcell-mediated transfer of a human chromosome 11 (including the *MRE11A* locus) into the cells from Patient 2 restored radiation sensitivity. (b) Formation of MRE11 and NBS1 radiation-induced nuclear foci. Cells were analyzed by immuno-staining at 24 h after 6 Gy irradiation. Normal cells served as a control, and NBS cells served as an *NBN*-deficient reference. MRE11 and NBS1 formed nuclear foci after irradiation in normal cells. In contrast, cells from Patients 1 and 2 showed only very faint signals.

transcripts from the c.338G allele of Patient 2 showed 25% of the normal level (Fig. 2d). By contrast, the transcript levels from the c.338G allele of the father were not affected. The c.338A>G substitution was not detected in 100 normal Japanese individuals.

3.2. *Cells from Patients 1 and 2 exhibit radiation-hypersensitivity*

A clonogenic radiation sensitivity assay was performed on fibroblast cells from Patients 1 and 2 on ATLD and A–T cells as references, and on normal cells as a control. The cells from Patients 1 and 2, and ATLD were hypersensitive to X-ray irradiation, as measured by the share of surviving fractions after irradiation (Fig. 3a). A–T cells showed more marked radiation-hypersensitivity than in Patients 1 and 2, and ATLD. We introduced chromosome 11 (containing the *MRE11A* locus) into the cells from Patient 2 through microcell-mediated transfer [12]. Two microcell-hybrid clones obtained and both showed restoration of radiation-sensitivity (Fig. 3a).

Next, we studied MRE11 and NBS1 radiation-induced nuclear foci formation 24 h after exposure to 6 Gy. MRE11 and NBS1 formed nuclear foci after irradiation in normal cells. In contrast, cells from Patients 1 and 2 showed only very faint signals of NBS1 and MRE11. It is noteworthy that a few NBS1 foci were present in Patient 1. These findings are likely to be compatible with the level of the protein in the cells (Fig. 3b).

Table 1
Chromosomal aberrations in lymphocytes after 2 Gy irradiation.

Cells	No. of cells analyzed	Chromosome aberrations			Total no. of aberrations	Chromosome aberrations per cell
		Chromatid break	Chromosome break	Quadriradial chromosome		
Normal	100	10	17	3	20	0.20
ATLD	100	12	46	64	122	1.22
Patient 1	105	20	64	47	178	1.70
Patient 2	100	66	65	67	198	1.98
A–T	100	62	102	34	198	1.98

Table 1 lists chromosomal aberrations induced by ionizing radiation in LCLs from Patients 1 and 2, ATLD and A–T. Chromosome aberrations scored included chromatid and chromosome breaks and quadriradials. Cells from Patients 1 and 2 both showed an increase of aberrations comparable to those in ATLD and A–T cells.

3.3. Cells from Patients 1 and 2 have levels of ATM activation higher than those in ATLD cells

We analyzed cells from Patients 1 and 2, A–T, and ATLD for radiation-induced ATM activation. ATM is phosphorylated at serine residue 1981 in response to irradiation [20]. We therefore gave 0.5 Gy of γ ray radiation to LCLs from Patients 1 and 2, A–T, and ATLD, and analyzed with Western blotting the intensity of their phosphorylated ATM bands. The LCLs from Patients 1 and 2 showed an increased intensity of the phosphorylated ATM band after irradiation, while very little ATM phosphorylation was observed at 0 and 15 min after irradiation in ATLD cells (200704L), and a phosphorylated band appeared only after 30 min (Fig. 4a). The fibroblast cells of Patients 1 and 2, and ATLD (D6807SVT) showed responses similar to the LCLs (Fig. 4b).

3.4. Cells from Patients 1 and 2 have G2/M checkpoint defects, and levels of p53 and caspase 3 activation higher than those in ATLD cells

Mitotic index was examined in the cells irradiated with 2 Gy of γ ray in order to monitor the ATM-dependent G2/M checkpoint. Fibroblasts from Patients 1 and 2, and ATLD (D6807SVT) 30 min after irradiation all showed a slight decrease in mitotic index, intermediate between control and A–T cells. At 2 h after irradiation, cells from Patients 1 and 2 showed a decrease of mitotic index to the level of normal cells, while ATLD cells showed a response intermediate between the control and A–T cells (Fig. 5a).

We studied phosphorylation of p53, an ATM substrate, in the LCLs from Patients 1 and 2, A–T, and ATLD. The LCLs from Patients 1 and 2 showed an increase of p53 phosphorylation at serine residue 15 after irradiation, whereas ATLD cells showed a noticeably small increase of p53 phosphorylation (Fig. 5b). We also studied caspase 3 activation in the cells from Patients 1 and 2, A–T, and ATLD as an endpoint of ATM-dependent apoptosis by Western blotting. Caspase 3 cleavage was apparent after irradiation in normal cells and Patients 1 and 2 cells, but not in A–T and ATLD cells (Fig. 5c).

4. Discussion

We have described two unrelated patients with severe microcephaly resembling Nijmegen breakage syndrome (NBS). NBS is a hereditary disorder caused by biallelic mutations of the *NBN* gene [7–9]. It is characterized by severe microcephaly, a bird-like facial appearance, growth and mental retardation, chromosomal instability, and cellular radiosensitivity [21]. The two patients we described both had all these features, but they showed neither immunodeficiency nor cancer predisposition, as is typical of NBS. We sequenced the *NBN*, *MRE11A*, and *RAD50* coding sequences in both patients, and found only the *MRE11A* mutations. Patient 1 had c.658A>C substitution plus a splicing mutation in the *MRE11A* gene, and Patient 2 had c.658A>C substitution and c.338A>G substitution. The c.658A>C substitution common to both patients resulted in a reduced level of normally functioning MRE11 protein. On the other hand, the c.338A>G substitution in Patient 2 resulted in a reduced level of MRE11 protein with a single amino acid substitution in the highly conserved domain. Therefore, the splicing mutation in

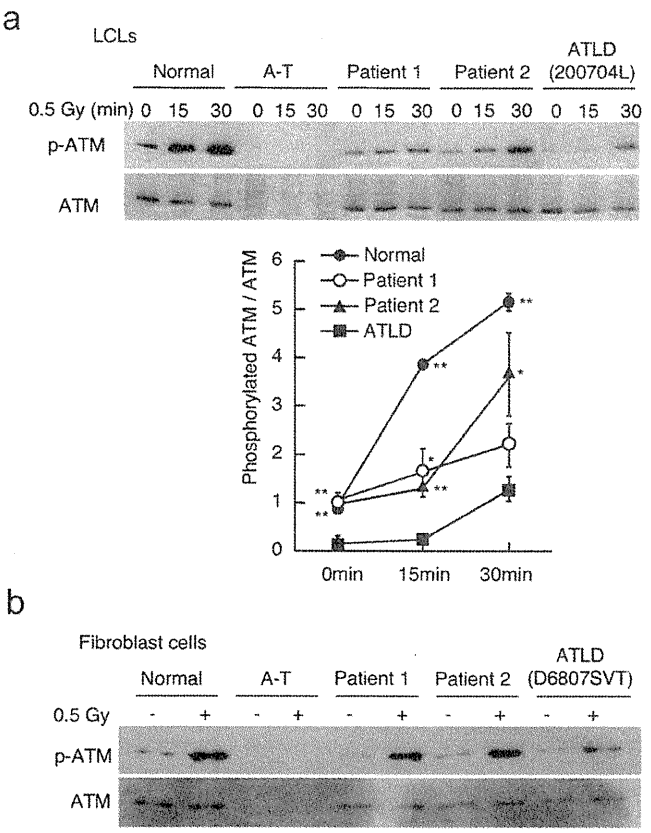

Fig. 4. Radiation-induced ATM activation. (a) Western blot analysis of phosphorylated ATM protein after irradiation of LCLs with 0.5 Gy γ ray. A–T cells served as an ATM-deficient cell line, and ATLD LCL (200704L) was used as a control. Phosphorylated ATM in LCLs from both Patients 1 and 2 increased after irradiation, while ATLD cells did not. ATLD LCL (200704L) was derived from a compound heterozygote for a *MRE11A* missense mutation (p.Trp243Arg) and a splicing mutation that resulted in exon 10 skipping, leading to an in-frame deletion (p.340–366del27) without correctly spliced transcripts [15]. The statistical significance of the differences in phosphorylated ATM/total ATM was examined by *t*-test. $^{*}p < 0.05$; $^{**}p < 0.01$ (normal, Patient 1, or Patient 2 versus ATLD). The data are shown as average ± standard error determined from three separate experiments. (b) Western blots of phospohrylated ATM protein at 30 min after irradiation of fibroblasts with 0.5 Gy of γ ray. A–T cells served as an ATM-deficient cell line, and ATLD fibroblasts (D6807SVT) harboring homozygous nonsense mutations were used as a control. Phosphorylated ATM in fibroblasts from both Patients 1 and 2 increased after irradiation, whereas ATLD cells did not.

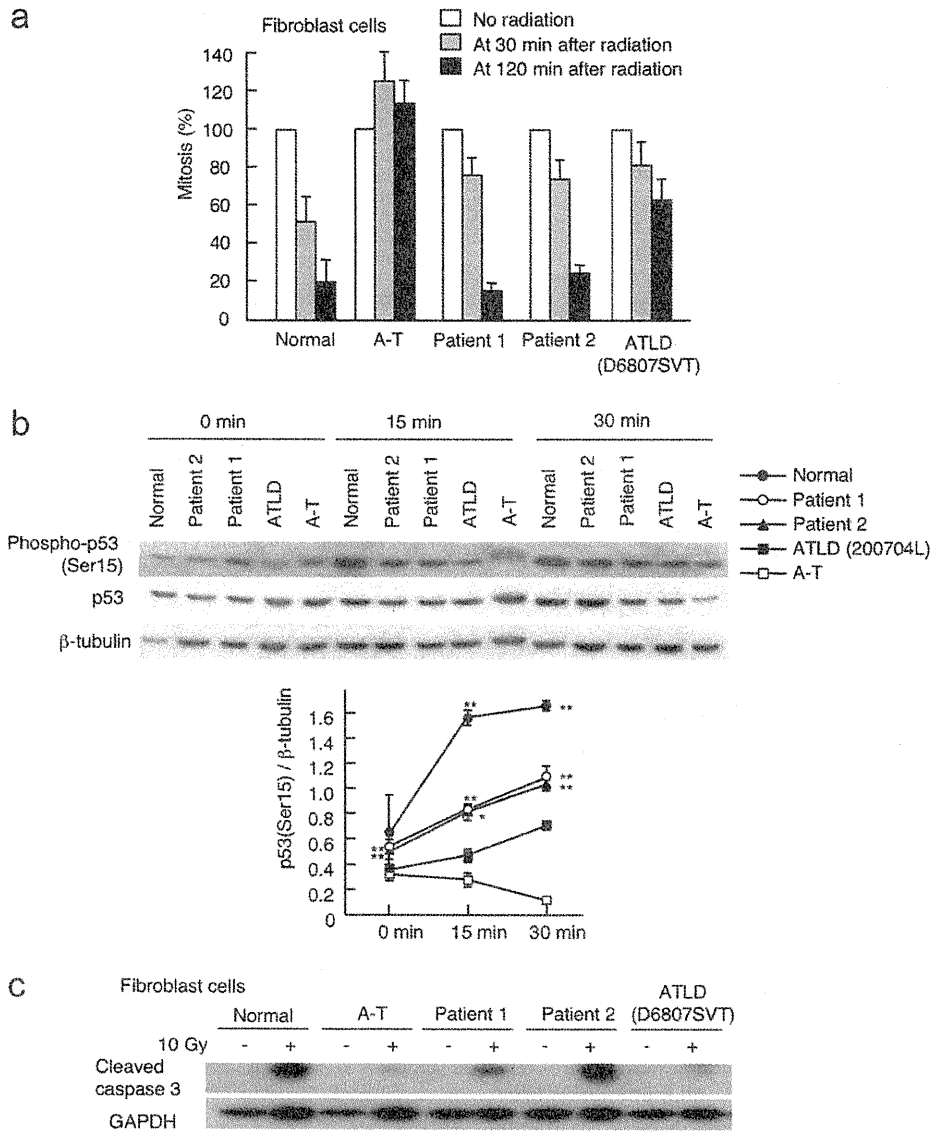

Fig. 5. Radiation-induced G2/M checkpoint and, p53 phosphorylation and caspase 3 activation as indicators of ATM activation deficiency. (a) Ataxia–telangiectasia (A–T) fibroblasts were used as an ATM-deficient reference, and ATLD fibroblasts (D6807SVT) harboring homozygous nonsense mutations were used as a control. Cultured fibroblast cells on a slide were irradiated with 2 Gy of γ ray, and stained 30 min or 2 h later with DAPI and rabbit anti-phospho-histone H3 polyclonal antibody. Mitotic index in each cell line without irradiation was estimated as 100%. Fibroblasts from Patients 1 and 2, and ATLD cells all showed a slight decrease in mitotic index at 30 min after irradiation, intermediate between normal and A–T cells. At 2 h after irradiation, cells from Patients 1 and 2 showed a decrease of mitotic index to the level of the normal cells, while ATLD cells showed a response intermediate between normal and A–T cells. Each column represents an average ± standard error from three separate experiments. (b) Western blots of phospohrylated p53 protein after irradiation. A–T and ATLD cells were used as controls. LCLs were irradiated with 0.5 Gy of γ ray. At 15 min and 30 min after irradiation, the cells were analyzed with Western blotting using rabbit anti-phosphorylated p53 (Ser15) polyclonal antibody (1:1000, Cell Signaling Technology, Beverly, MA) and mouse anti-p53 monoclonal antibody (1:1000, Oncogene Research Products, CA). Phosphorylated p53 in LCLs from Patients 1 and 2 increased after irradiation, whereas such an increase was smaller in ATLD cells. The statistical significance of the differences in phosphorylated p53/β-tubulin was tested by *t*-test. $^{*}p < 0.05$; $^{**}p < 0.01$ (normal, Patient 1, or Patient 2 versus ATLD). The data are shown as average ± standard error determined from three separate experiments. (c) Western blot analysis of cleaved caspase 3 protein after 10 Gy γ-irradiation of fibroblast cells. Cleaved caspase 3 bands were seen in normal, Patients 1 and 2 cells, but not in A–T and ATLD cells.

Patient 1 and the missense mutation in Patient 2 were assumed to be functionally debilitating.

MRE11A is known as the gene underlying ataxia–telangiectasia-like disorder (ATLD), a milder and slowly progressive variant of A–T without microcephaly [5]. To date, seven families with ATLD patients have been reported: two in the U.K., one in Italy, three in Saudi Arabia, and one in Japan. These patients with *MRE11A* mutations included: compound heterozygotes with a splicing mutation plus a missense mutation; homozygotes for a missense mutation; compound heterozygotes with a missense mutation plus a nonsense mutation; and homozygotes for a nonsense mutation.

It was reported that the MRE11/RAD50/NBS1 protein complex is involved in radiation-induced ATM activation [14]. We therefore analyzed level of radiation-induced ATM activation in cells from Patients 1 and 2, and those from ATLD patients. Cells from Patients 1 and 2 showed the level of ATM activation higher than those in ATLD cells. The cells from Patients 1 and 2 both showed the levels of p53 phosphorylation and caspase-3 activation higher than those in ATLD cells. The differences are likely to be attributable to the presence of normally functioning MRE11 protein in Patients 1 and 2.

Several explanations are conceivable for the unusual clinical features in the two patients. First, ATM-dependent neuronal apop-

tosis has been proposed as a mechanism underlying microcephaly in DNA damage disorders [2,22–24]. According to this model, the two patients might have undergone extensive neuronal apoptosis during development due to the relatively higher level of ATM activation, and developed severe microcephaly, while ATLD patients cannot activate ATM, thereby failing to engage in apoptosis but presenting with neurodegeneration. The second possibility is that the effect of microcephaly might be mediated through NBS1. Since *MRE11A* mutations often affect the levels of NBS1 and RAD50, and NBS1 deficiency uniformly leads to microcephaly, the effect of these *MRE11A* mutations might be indirect and those that result in greater diminution in the levels of NBS1 might be more prone to microcephaly. The third possibility is that an additional gene(s) other than *MRE11A* might be involved in development of microcephaly. The molecular mechanism underlying neuropathology remains to be elucidated.

In conclusion, we have identified and characterized the two patients with *MRE11A* mutations but severe microcephaly. This report suggests that MRE11 deficiency has a wider spectrum of the clinical features than that has been thought.

Conflict of interest statement

There is no conflict of interest.

Acknowledgements

We thank the families for their cooperation in the study, Drs. S. Nonoyama and K. Imai for providing ATLD cells, Dr. K. Sperling for NBS cells, Dr. M. Oshimura for a mouse hybrid cell line, Drs. J. Kobayashi and T. Ishii for discussion, Dr. M. Kobayashi for providing clinical information, and Ms. Y. Tonouchi for assistance. We thank Dr. T. Kajii for critically reading the manuscript. This work was supported by Grants-in-Aid for Scientific Research from the Ministry of Education, Culture, Sports, Science and Technology.

References

[1] A. Kulkarni, D.M. Wilson 3rd, The involvement of DNA-damage and -repair defects in neurological dysfunction, Am. J. Hum. Genet. 82 (2008) 539–566.
[2] M. O'Driscoll, P.A. Jeggo, The role of the DNA damage response pathways in brain development and microcephaly: insight from human disorders, DNA Repair (Amst.) 7 (2008) 1039–1050.
[3] M.F. Lavin, ATM and the Mre11 complex combine to recognize and signal DNA double-strand breaks, Oncogene 26 (2007) 7749–7758.
[4] M.F. Lavin, Ataxia–telangiectasia: from a rare disorder to a paradigm for cell signalling and cancer, Nat. Rev. Mol. Cell Biol. 9 (2008) 759–769.
[5] A.M. Taylor, A. Groom, P.J. Byrd, Ataxia–telangiectasia-like disorder (ATLD) – its clinical presentation and molecular basis, DNA Repair (Amst.) 3 (2004) 1219–1225.
[6] G.S. Stewart, R.S. Maser, T. Stankovic, D.A. Bressan, M.I. Kaplan, N.G. Jaspers, A. Raams, P.J. Byrd, J.H. Petrini, A.M. Taylor, The DNA double-strand break repair gene hMRE11 is mutated in individuals with an ataxia–telangiectasia-like disorder, Cell 99 (1999) 577–587.
[7] S. Matsuura, H. Tauchi, A. Nakamura, N. Kondo, S. Sakamoto, S. Endo, D. Smeets, B. Solder, B.H. Belohradsky, V.M. Der Kaloustian, M. Oshimura, M. Isomura, Y. Nakamura, K. Komatsu, Positional cloning of the gene for Nijmegen breakage syndrome, Nat. Genet. 19 (1998) 179–181.
[8] J.P. Carney, R.S. Maser, H. Olivares, E.M. Davis, M. Le Beau, J.R. Yates 3rd, L. Hays, W.F. Morgan, J.H. Petrini, The hMre11/hRad50 protein complex and Nijmegen breakage syndrome: linkage of double-strand break repair to the cellular DNA damage response, Cell 93 (1998) 477–486.
[9] R. Varon, C. Vissinga, M. Platzer, K.M. Cerosaletti, K.H. Chrzanowska, K. Saar, G. Beckmann, E. Seemanova, P.R. Cooper, N.J. Nowak, M. Stumm, C.M. Weemaes, R.A. Gatti, R.K. Wilson, M. Digweed, A. Rosenthal, K. Sperling, P. Concannon, A. Reis, Nibrin, a novel DNA double-strand break repair protein, is mutated in Nijmegen breakage syndrome, Cell 93 (1998) 467–476.
[10] R. Waltes, R. Kalb, M. Gatei, A.W. Kijas, M. Stumm, A. Sobeck, B. Wieland, R. Varon, Y. Lerenthal, M.F. Lavin, D. Schindler, T. Dork, Human RAD50 deficiency in a Nijmegen breakage syndrome-like disorder, Am. J. Hum. Genet. 84 (2009) 605–616.
[11] S.A. Carney, H. Tahara, C.D. Swartz, J.I. Risinger, H. He, A.B. Moore, J.K. Haseman, J.C. Barrett, D. Dixon, Immortalization of human uterine leiomyoma and myometrial cell lines after induction of telomerase activity: molecular and phenotypic characteristics, Lab. Invest. 82 (2002) 719–728.
[12] S. Matsuura, C. Weemaes, D. Smeets, H. Takami, N. Kondo, S. Sakamoto, N. Yano, A. Nakamura, H. Tauchi, S. Endo, M. Oshimura, K. Komatsu, Genetic mapping using microcell-mediated chromosome transfer suggests a locus for Nijmegen breakage syndrome at chromosome 8q21–24, Am. J. Hum. Genet. 60 (1997) 1487–1494.
[13] K. Komatsu, S. Kodama, Y. Okumura, M. Koi, M. Oshimura, Restoration of radiation resistance in ataxia telangiectasia cells by the introduction of normal human chromosome 11, Mutat. Res. 235 (1990) 59–63.
[14] T. Uziel, Y. Lerenthal, L. Moyal, Y. Andegeko, L. Mittelman, Y. Shiloh, Requirement of the MRN complex for ATM activation by DNA damage, EMBO J. 22 (2003) 5612–5621.
[15] N. Uchisaka, N. Takahashi, M. Sato, A. Kikuchi, S. Mochizuki, K. Imai, S. Nonoyama, O. Ohara, F. Watanabe, S. Mizutani, R. Hanada, T. Morio, Two brothers with ataxia–telangiectasia-like disorder with lung adenocarcinoma, J. Pediatr. 155 (2009) 435–438.
[16] S.A. Pitts, H.S. Kullar, T. Stankovic, G.S. Stewart, J.I. Last, T. Bedenham, S.J. Armstrong, M. Piane, L. Chessa, A.M. Taylor, P.J. Byrd, hMRE11: genomic structure and a null mutation identified in a transcript protected from nonsense-mediated mRNA decay, Hum. Mol. Genet. 10 (2001) 1155–1162.
[17] J. Kobayashi, H. Tauchi, S. Sakamoto, A. Nakamura, K. Morishima, S. Matsuura, T. Kobayashi, K. Tamai, K. Tanimoto, K. Komatsu, NBS1 localizes to gamma-H2AX foci through interaction with the FHA/BRCT domain, Curr. Biol. 12 (2002) 1846–1851.
[18] E. Griffith, S. Walker, C.A. Martin, P. Vagnarelli, T. Stiff, B. Vernay, N. Al Sanna, A. Saggar, B. Hamel, W.C. Earnshaw, P.A. Jeggo, A.P. Jackson, M. O'Driscoll, Mutations in pericentrin cause Seckel syndrome with defective ATR-dependent DNA damage signaling, Nat. Genet. 40 (2008) 232–236.
[19] R.S. Williams, G. Moncalian, J.S. Williams, Y. Yamada, O. Limbo, D.S. Shin, L.M. Groocock, D. Cahill, C. Hitomi, G. Guenther, D. Moiani, J.P. Carney, P. Russell, J.A. Tainer, Mre11 dimers coordinate DNA end bridging and nuclease processing in double-strand-break repair, Cell 135 (2008) 97–109.
[20] C.J. Bakkenist, M.B. Kastan, DNA damage activates ATM through intermolecular autophosphorylation and dimer dissociation, Nature 421 (2003) 499–506.
[21] S. Matsuura, J. Kobayashi, H. Tauchi, K. Komatsu, Nijmegen breakage syndrome and DNA double strand break repair by NBS1 complex, Adv. Biophys. 38 (2004) 65–80.
[22] P.O. Frappart, W.M. Tong, I. Demuth, I. Radovanovic, Z. Herceg, A. Aguzzi, M. Digweed, Z.Q. Wang, An essential function for NBS1 in the prevention of ataxia and cerebellar defects, Nat. Med. 11 (2005) 538–544.
[23] C. Barlow, K. Treuner, DNA instability in the brain: survival of the 'fittest', Nat. Med. 11 (2005) 474–475.
[24] E.R. Shull, Y. Lee, H. Nakane, T.H. Stracker, J. Zhao, H.R. Russell, J.H. Petrini, P.J. McKinnon, Differential DNA damage signaling accounts for distinct neural apoptotic responses in ATLD and NBS, Genes Dev. 23 (2009) 171–180.

Hum Genet (2012) 131:121–130
DOI 10.1007/s00439-011-1051-4

ORIGINAL INVESTIGATION

Spread of X-chromosome inactivation into chromosome 15 is associated with Prader–Willi syndrome phenotype in a boy with a t(X;15)(p21.1;q11.2) translocation

Satoru Sakazume · Hirofumi Ohashi · Yuki Sasaki · Naoki Harada · Katsumi Nakanishi · Hidenori Sato · Mitsuru Emi · Kazushi Endoh · Ryoichi Sohma · Yasuhiro Kido · Toshiro Nagai · Takeo Kubota

Received: 25 February 2011 / Accepted: 19 June 2011 / Published online: 7 July 2011

Abstract X-chromosome inactivation (XCI) is an essential mechanism in females that compensates for the genome imbalance between females and males. It is known that XCI can spread into an autosome of patients with X;autosome translocations. The subject was a 5-year-old boy with Prader–Willi syndrome (PWS)-like features including hypotonia, hypo-genitalism, hypo-pigmentation, and developmental delay. G-banding, fluorescent in situ hybridization, BrdU-incorporated replication, human androgen receptor gene locus assay, SNP microarrays, ChIP-on-chip assay, bisulfite sequencing, and real-time RT-PCR were performed. Cytogenetic analyses revealed that the karyotype was 46,XY,der(X)t(X;15)(p21.1;q11.2),−15. In the derivative chromosome, the X and half of the chromosome 15 segments showed late replication. The X segment was maternal, and the chromosome 15 region was paternal, indicating its post-zygotic origin. The two chromosome 15s had a biparental origin. The DNA methylation level was relatively high in the region proximal from the breakpoint, and the level decreased toward the middle of the chromosome 15 region; however, scattered areas of hypermethylation were found in the distal region. The promoter regions of the imprinted *SNRPN* and the non-imprinted *OCA2* genes were completely and half methylated, respectively. However, no methylation was found in the adjacent imprinted gene *UBE3A*, which contained a lower density of LINE1 repeats. Our findings suggest that XCI spread into the paternal chromosome 15 led to the aberrant hypermethylation of *SNRPN* and *OCA2* and their decreased expression, which contributes to the PWS-like features and hypo-pigmentation of the patient. To our knowledge, this is the first chromosome-wide methylation study in which the DNA methylation level is demonstrated in an autosome subject to XCI.

Electronic supplementary material The online version of this article (doi:10.1007/s00439-011-1051-4) contains supplementary material, which is available to authorized users.

S. Sakazume (✉) · R. Sohma · Y. Kido · T. Nagai
Division of Pediatrics, Dokkyo University Koshigaya Hospital, 2-1-50 Minami Koshigaya, Koshigaya, Saitama 343-8555, Japan
e-mail: saka343@dokkyomed.ac.jp

H. Ohashi
Division of Genetics, Saitama Children's Medical Center, Hasuda, Japan

Y. Sasaki · N. Harada
Department of Molecular Genetic Research and Analysis, Advanced Medical Science Research Center, Mitsubishi Chemical Medience Corporation, Tokyo, Japan

K. Nakanishi · H. Sato · M. Emi
DNA Chip Research Inc, Yokohama, Japan

H. Sato · M. Emi
Department of Neurology, Hematology, Metabolism, Endocrinology and Diabetology, Yamagata University School of Medicine, Yamagata, Japan

K. Endoh · T. Kubota
Department of Epigenetic Medicine, Faculty of Medicine, Interdisciplinary Graduate School of Medicine and Engineering, University of Yamanashi, Chuo, Japan

Introduction

X-chromosome inactivation (XCI) is a genetic mechanism in females in which one of the two X chromosomes are stochastically inactivated in the early stages of embryonic development. In each cell, the inactivated X-chromosome is randomly chosen; therefore, paternal and maternal X chromosomes have a 50% probability of being inactivated, and females are functional mosaic of two cell populations (Lyon 1961, 1962).

XCI is an essential mechanism for normal development that contributes to gene-dosage compensation process in females (Takagi and Abe 1990). Failure of XCI in females leads to embryonic lethality or abortion on the basis of observations in the embryos of cloned animals (Xue et al. 2002; Yang et al. 2007) or severe phenotypes at birth in humans (Schmidt and Du Sart 1992; Kubota et al. 2002). X-inactivation is mediated by the X inactive-specific transcript gene (*XIST*), a cis-acting RNA molecule (Brown et al. 1991). Studies using ectopic mouse *Xist* integrated into an autosome have demonstrated that *Xist* RNA coats the transgenic autosomes, leading to the reduced expression of genes over 50 cM, and suggest that long-range cis effects occur on the autosome (Herzing et al. 1997; Lee and Jaenisch 1997; Lee et al. 1996). In this report, we describe a boy with t(X;15)(p21.1;q11.2), and analyze the breakpoints, status of the *XIST* gene, extent of XCI spread on an autosome using the DNA methylation status at the CpG islands of genes related to the patient's clinical features. To date, only three studies have measured the spread of X inactivation by gene expression analysis using a somatic cell hybrid that carries the translocated chromosome (Giorda et al. 2008; White et al. 1998) or allele-specific quantitative RT-PCR using heterozygous polymorphism (Sharp et al. 2002). In this report, we investigate how XCI spreads in an autosome using a microarray-based method. To our knowledge, this is the first report that demonstrates the level and extent of XCI in an autosome at a chromosome-wide level in terms of DNA methylation.

Methods

Chromosome and fluorescent in situ hybridization (FISH) analyses

High-resolution G-banded chromosomes were prepared from peripheral blood lymphocytes according to standard procedures. FISH using bacterial artificial chromosome (BAC) DNA as a probe was performed on metaphase chromosomes of the patient with der (X). Chromosome slides were pre-incubated in 2× SSC at 37°C for 30 min, denatured in 70% formamide with 2× SSC at 72°C for 2 min, and then dehydrated at −20°C in ethanol. Cloned DNA was labeled with SpectrumGreen TM-11-dUTP or SpectrumOrange TM-11-dUTP (Vysis, Downers Grove, IL, USA) by nick translation and denatured at 76°C for 10 min. The probe-hybridization mixture (10 mL) was applied to the chromosomes, and they were incubated at 37°C for 16 h. Slides were washed three times in 4× SSC, 0.1% Tween-20 at 45°C and mounted in an anti-fade solution (Vector, Burlingame, CA, USA) containing DAPI.

We used 32 BAC clones to confirm the break point of the X chromosome and to confirm the presence of the *XIST* gene in the der (X). We also used 12 BAC clones to confirm the breakpoint of chromosome 15. The BAC clones, their locations, and the containing gene are shown in Supplemental Table 1. All of the clones were selected using the UCSC genome browser database (http://genome.ucsc.edu).

Quantitative RT-PCR analysis

Total RNA was isolated using the RNeasy Mini Kit (Qiagen, Hilden, Germany) according to the manufacturer's instruction. Reverse transcription and real-time RT-PCR were carried out using SYBR ExScript RT-PCR Kit (Takara, Kyoto, Japan). Quantitative real-time RT-PCR analysis was performed in triplicate with an Applied Biosystems (Foster City, CA, USA) Prism 7700 Sequence detection system according to the manufacturer's instructions. The mRNA expression levels, normalized against those of the corresponding *GAPDH* mRNA levels, were relatively quantified. The primer pairs used for the *GAPDH* and *OCA2* genes were GAPDH (HA031578, Takara) and OCA2 (HA032005, Takara), respectively, and the primer sequences for the *XIST* gene were: XIST-113202F, 5′-GCAGTTTGCCCTACTAGCTCCT-3′ and XIST-11456R, 5′-TCCTCAGGTCTCACATGCTCA-3′.

X-chromosome inactivation analyses

Replication R-banding study was performed on chromosomes stained with DAPI as described elsewhere (Uehara et al. 2001).

The human androgen receptor gene locus (HUMARA) assay using methylation-specific PCR was performed as described previously (Kubota et al. 1999). Briefly, the assay uses a bisulfite-treatment followed by PCR, and we obtained the inactive X pattern based on the methylated allele at the HUMARA locus and the active X pattern based on the unmethylated allele at the same locus. Both patterns were used to calculate the XCI ratio (Kubota et al. 1999).

Methylated DNA immunoprecipitation (MeDIP) assay using a human CpG island microarray

The methylation status of the CpG islands (CGIs) was analyzed using the methylated DNA immunoprecipitation method with a human CGI oligonucleotide microarray system according to the manufacturer's protocol (Agilent Technologies, Santa Clara, CA, USA). Briefly, sonicated genomic DNA was prepared and used for immunoprecipitation with a 5-methylcytidine monoclonal antibody (BI-MECY-1000) (Eurogentec, Seraing, Belgium). We

labeled 250 ng of methylation-enriched DNA samples and reference (input, non-enriched control) DNA samples, which were not amplified, with Cy3 and Cy5, respectively, using an Agilent Genomic DNA Labeling Kit PLUS (Agilent Technologies). Labeled DNA was hybridized to the custom array containing 5,859 high-density probes specific for the CpG promoters on chromosome 15, which was designed using the eArray Agilent web-based database (hg18, NCBI 36.3) on a 44K platform CpG promoter microarray. The array was scanned with an Agilent G2565BA microarray scanner (Agilent Technologies). All experiments were performed in duplicate. We compared methylation between the patient and two normal controls, according to the previously described methodology (Sharp et al. 2010).

Bisulfite DNA sequencing

Genomic DNA was extracted from peripheral lymphocytes, and bisulfite treatment of genomic DNA was performed using the EpiTect Bisulfite Kit (Qiagen) according to the manufacturer's instructions. Primers for the bisulfite genomic sequencing PCR were designed using the online program MethPrimer (http://www.urogene.org/methprimer/index1.html). The amplified PCR products were sequenced using the following primers:

SNRPN-F, 5′-AAAAACTTTAAAACCCAAATTCC-3′;
SNRPN-R, 5′-GTGGGGTTTTAGGGGTTTAGTA-3′;
UBE3A-F, 5′-TTCTAACACCAACCCCTTC-3′;
UBE3A-R, 5′-AGTTTTTY (C and T) GGTGTGGATA GGTA-3′;
OCA2-F, 5′-TGTGTTTGTGTTGTAGGAGGGGT-3′;
OCA2-R, 5′-CCCACAAAACTACCCACATAACC-3′;
UBR1-F, 5′-AATATTTTTTGGGGTTTGTAGGT GA-3′;
UBR1-R, 5′-CAAAACCAACACTAAACAAAACCT C-3′;
TRIP15-F, 5′-GAAAGGGTAAAGTTAGGGTTTAT AT-3′;
and TRIP15-R, 5′-CCTACTTCTCCAACAAAAAAA AA-3′.

Single nucleotide polymorphism (SNP) analysis using a microarray

SNPs on chromosome 15 were analyzed using the Human 317K-Duo Bead chip array, and SNP genotypes were determined using the GenomeStudio software (Illumina, San Diego, CA, USA). More than 317,000 tagSNPs markers on this chip were selected using the database of the International HapMap Project Phase I and Phase II (NCBI build 36.3/hg18).

Genomic search for transposable elements

The UCSC data (NCBI 36.3/hg18) were searched for LINE1 (L1), Mammalian-wide Interspersed Repeat (MIR), and Alu transposable elements using the RepeatMasker Program (Ver. 3.2.7). We focused on the *SNRPN*, *UBE3A*, and *OCA2* genes, and plotted the elements using the R program (Ver. 2.10).

Results

Proband

The male proband was a 5-year-old boy and the only child of healthy and non-consanguineous parents. The pregnancy was not eventful and he was born at the 41st week of gestation and weighed 2,933 g. Body length and head circumference were at the 50th percentile (49 and 35.5 cm, respectively). Hypotonia was prominent and nasogastric tube was required for feeding during the neonatal period. PWS-like dysmorphic features were noted, including small mouth, micrognathia, rocker-bottom feet, hypopigmented hair, cryptorchidism, and hypogenitalism. Abdominal ultrasound revealed a horseshoe kidney, while head MRI demonstrated hypo-plastic corpus callosum and occipital arachnid cyst. He had severe motor developmental delay and spastic quadriplegia: at the age of 20 months he could not control his head and could not roll over. A wheelchair was required to move and continuous drainage of saliva was necessary due to difficulties with swallowing.

Cytogenetic analysis

High-resolution G-banding showed an abnormal karyotype: 46,XY,der(X)t(X;15),−15 in all 50 cells analyzed (Fig. 1a). Karyotypes of both parents were normal (data not shown). To confirm the break point of the derivative X chromosome in the patient, FISH analyses were performed, in which a series of BAC probes to the X chromosome were hybridized on metaphase spreads of the patient's lymphocytes. As a result, the signals from the RP11-172M3 probe (SpectrumOrange), mapping to Xp21.2, and from RP11-134B11 (SpectrumGreen), mapping to Xp21.1, were detected on the normal X chromosome, whereas only signal from RP11-134B11 (SpectrumGreen), mapping to Xp21.1, was detected on the derivative X chromosome, indicating that the break point of the derivative X was located between these probes (Xp21.2-p21.1 region) (Fig. 1b). Likewise, the signals from the RP11-79C23 probe (SpectrumOrange), mapping to 15q11.1-11.2, and from RP11-357P4 (SpectrumGreen), mapping to 15q11.2, were detected on the normal chromosome 15, whereas only signal from RP11-357P41 (SpectrumGreen), mapping to 15q11.2, was detected on the

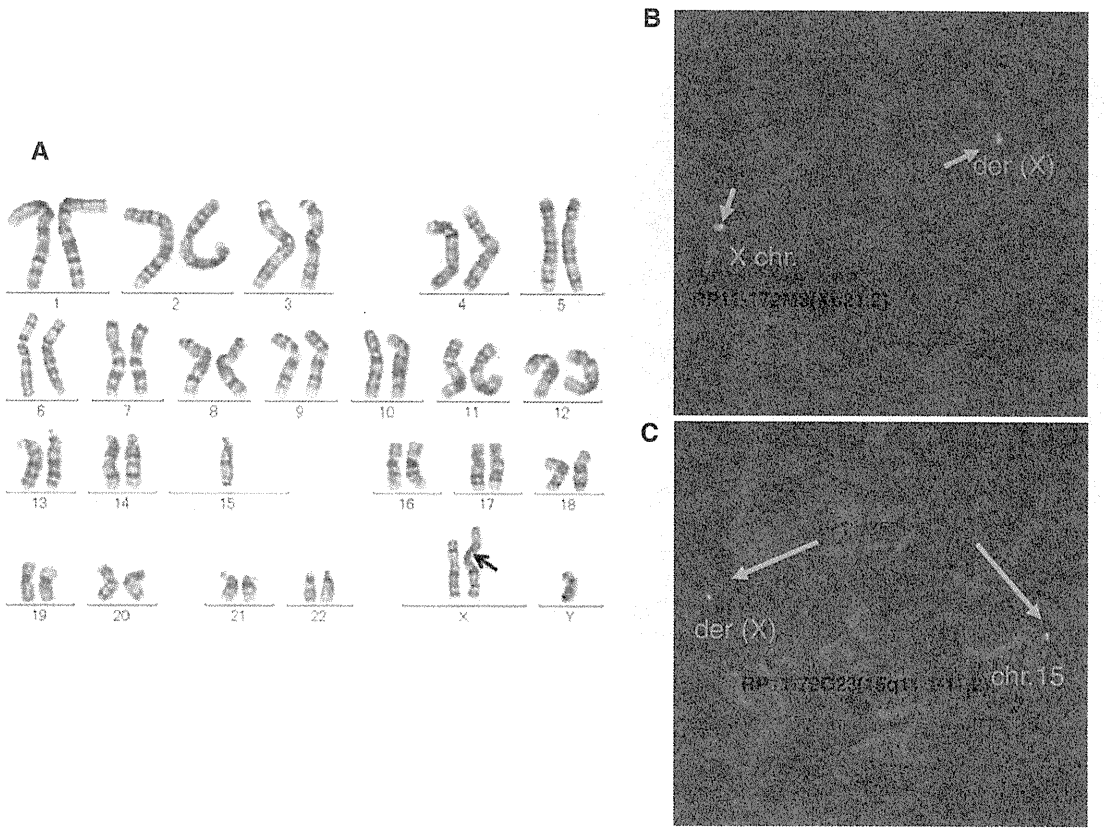

Fig. 1 Cytogenetic analyses of the patient. **a** GTG-banded full karyotype of the patient. No mosaicism was found in the 50 cells examined. An *arrow* indicates the breakpoint of the derivative X chromosome. **b** FISH analysis using the RP11-172M3 probe (SpectrumOrange) at Xp21.2 (a signal shown in *red*) and the RP11-134B11 probe (SpectrumGreen) at Xp21.1 (two signals shown in *green*). The presence of a *green* signal, but not a *red* signal, in the derivative X chromosome (der (X)) indicate that the breakpoint is located between the two probes (Xp21.2-p21.1). **c** FISH analysis using the RP11-79C23 probe (SpectrumOrange) at 15q11.1-q11.2 (a signal shown in *red*) and the RP11-357P4 probe (SpectrumGreen) at 15q11.2 (two signals shown in *green*). The presence of a *green* signal, but not a *red* signal, in the derivative X chromosome (der (X)) indicate that the breakpoint is located between the two probes (15q11.1-q11.2)

derivative X chromosome, indicating that the break point of the derivative X was located between these probes (15q11.2) (Fig. 1c). Taken together, the patient's karyotype was interpreted as 46,XY,der(X)t(X;15)(p21.1;q11.2),−15.

SNP analysis of chromosome 15

To determine the parental origin of the chromosomes 15 in the patient, we examined the 9303 SNPs on chromosome 15 and found that 444 SNPs demonstrated the biparental inheritance of chromosome 15 in the patient (Table S2). The remaining SNPs were uninformative and none showed uniparental origin. Since the SNRPN gene promoter region was extremely methylated, in which the normally unmethylated paternal allele was methylated presumably due to XCI, the chromosome 15 region in the derivative X was determined to be of paternal origin. Therefore, together with the results of the HUMARA assay, in which the normal X and derivative X chromosomes were maternal, SNP analysis suggests that the derivative X consisted of the maternal X chromosome and the paternal chromosome 15.

X-chromosome inactivation analysis

To examine the XCI status in the derivative X chromosome, we first performed FISH analysis with a BAC probe containing the *XIST* gene to confirm its presence. As a result, the signal from the BAC probe RP11-13M9 (SpectrumGreen) was retained in the normal and derivative X chromosomes, as was the signal from the X-chromosome control probe RP11-402H20 (SpectrumOrange) at the Xq subtelomeric region (Fig. 2a). Replication R banding analysis demonstrated that the derivative X chromosome was inactivated, and this inactivation covered the X chromosome and the proximal 15q region; however, the inactivation did not spread distal to 15q in all the 100 cells

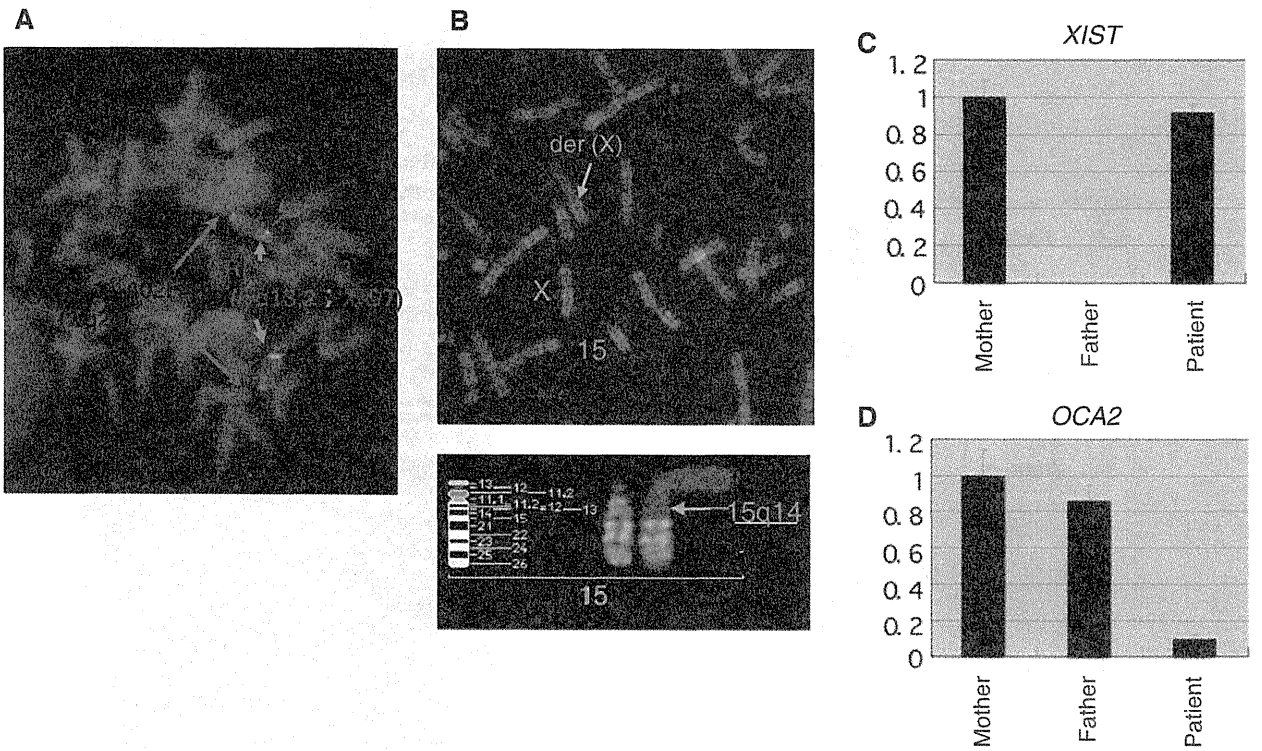

Fig. 2 Cytogenetic analysis for X-chromosome inactivation. **a** FISH analysis using the RP11-13M9 probe (SpectrumGreen), covering the *XIST* gene (two signals shown in *green*) and the RP11-402H20 probe (SpectrumOrange), located at the Xq-subtelomeric region (two signals shown in *red*), indicating that the derivative and normal X chromosomes have an *XIST* gene. **b** Replication R-banding study in the patient. A late replication/no banded segment was observed in the derivative X chromosome beyond the 15q14 region, which was assessed by the R-banding pattern of the normal chromosome 15 (see *lower enlarged panel*). **c** Real-time RT-PCR assay for *XIST* gene expression in the patient and parents. **d** Real-time RT-PCR assay for *OCA2* gene expression in the patient and parents. The *axis* represents the relative expression level for the mother (**c**, **d**)

examined (Fig. 2b, upper and lower panels with enlargement). We also confirmed *XIST* gene expression in the patient using real-time RT-PCR at almost the same level as in the mother, a normal female (Fig. 2c), suggesting *XIST* expression from the allele on the derivative X chromosome.

The HUMARA assay showed that the patient had a relatively non-random (skewed) XCI pattern (89:11) whereas the mother had a random XCI pattern (41:59). In addition, two copies of the HUMARA gene locus (Xq12) were inherited from the mother and no copy was inherited from the father (Fig. 3). These data indicate that the XIST gene was expressed from the derivative X, leading to the XCI effect spreading to the middle of the chromosome 15 in the derivative X beyond the break point, and also indicate that the normal and derivative X chromosomes were transmitted from the mother. The relatively skewed inactivation pattern in the patient was consistent with the result of the replication study, in which one X (presumably the derivative X) was preferentially inactivated in all cells examined.

DNA methylation analyses of CGIs on chromosome 15 of the derivative X chromosome

To further understand the spread of XCI on the chromosome 15 of the derivative X in terms of DNA methylation, we performed MeDIP analysis using CGI microarray to identify CGI hypermethylated regions in the patient in comparison with two healthy male controls (Fig. 4, upper panel). As a result, we observed constant CGI hypermethylation from the break point, beyond the *OCA2* locus (15q12), to 15q14 [40 Mb from the centromere]. In the middle of 15q, from 15q21.1 [50 Mb] to 15q22.2 [60 Mb], including *UBR1* (15q15.2) and *TRIP15* (15q21.1), CGI hypermethylation was rarely detected. However, scattered CGI hypermethylation was observed in the remaining telomeric region distal to 15q22.2 [60 Mb] in the patient (Fig. 4, upper panel).

In the proximal region, the CGIs of *SNRPN*, *ATP10A*, and *OCA2* were hypermethylated in the patient, whereas that of *UBE3A*, which was located in the middle of these

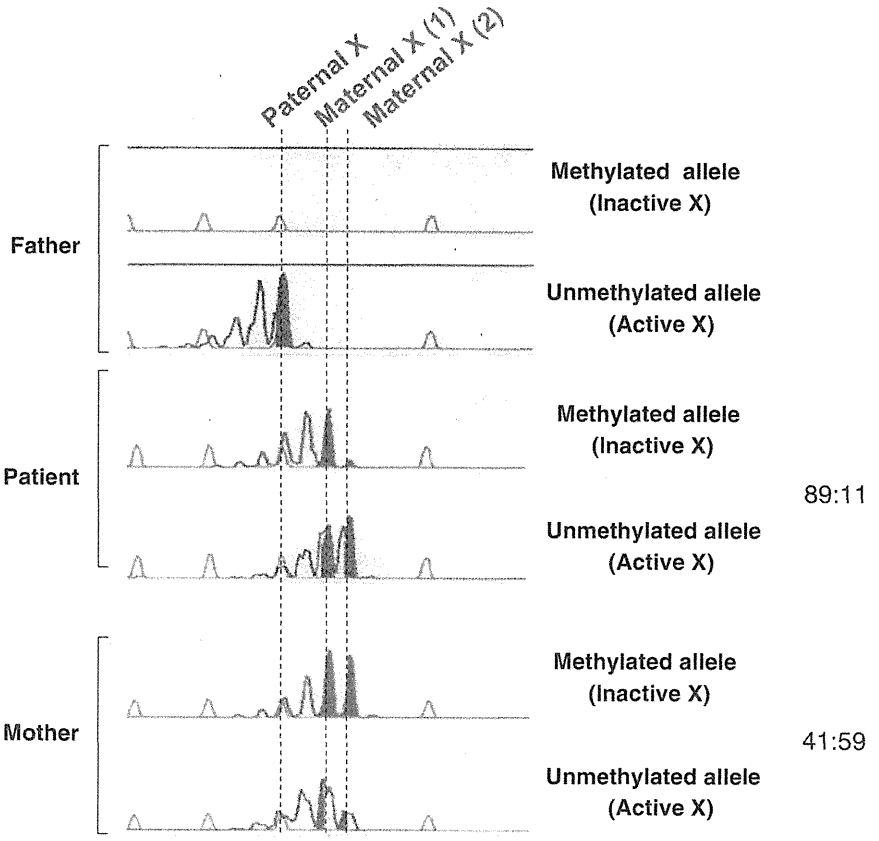

Fig. 3 Molecular analysis of X-chromosome inactivation. The HUMARA assay, based on methylation-specific PCR, demonstrates that the peak area of "Maternal X (1)" is much larger than that of "Maternal X (2)" in the methylated allele (Inactive X) lane in the patient, indicating relatively non-random (skewed) inactivation (89:11). However, the peak area of "Maternal X (1)" is affected by a shadow peak of "Maternal X (2)" in the unmethylated allele (Active X) lane, by PCR slippage error at the triplet repeat locus, because the allele difference between "Maternal X (1)" and "Maternal X (2)" is only 3 base pairs (1 triplet). Therefore, in this case, we only consider the result in the methylated allele (Inactive X) lane. In the mother, the patterns of the peak area of "Maternal X (1)" and "Maternal X (2)" are similar between the methylated (Inactive X) and unmethylated allele (Active X) lanes, indicating random inactivation (41:59). In the father, no peak is detected in the methylated allele (Inactive X) lane and only 1 peak is detected in the unmethylated allele (Active X) lane, as expected

genes, was not hypermethylated (Fig. 4, middle panel). In the middle region, the CGIs of *UBR1* and *TRIP15* were not hypermethylated in the patient (Fig. 4, middle panel).

Bisulfite sequencing analyses confirmed the results obtained from the MeDIP analysis. The CGI of *SNRPN* was extensively hypermethylated in the patient, whereas a healthy control showed ~50% methylation. Since *SNRPN* is an imprinted gene in which only the maternal allele is hypermethylated, this observation suggests that the normally unmethylated paternal allele (presumably the allele on the derivative X) was methylated in the patient (Fig. 3, lower panel). In the CGI of *OCA2*, the patient showed ~50% methylation whereas the control was not methylated, indicating that one of the two alleles (presumably the allele on the derivative X) was hypermethylated in the patient (Fig. 4, lower panel). This observation was consistent with the lower expression level of this gene in the patient (Fig. 2e). Taken together, the CGIs of the genes at 15q11.2-12 were hypermethylated presumably due to the spread of XCI in the derivative X.

However, the CGI of *UBE3A* was not shown to be hypermethylated by either the microarray assay or bisulfite sequencing analysis (Fig. 4, middle and lower panels); however, CGIs of the adjacent genes, *SNRPN* and *ATP10A*, were hypermethylated (Fig. 4, middle panel), indicating that the CGI of *UBE3A* might have some mechanism to escape the X-inactivation effect. We observed a lower density of LINE-1 and Alu elements in the upstream region of UBE3A (GenBank Accession No.: NM_000462) (Fig. 4, light blue area) compared with that in the upstream region of SNRPN (GenBank Accession No.: NM_003097) (Fig. 5, light pink area). As for MIR elements, no difference was found between these regions and both regions only contained a few MIR elements (Fig. 5).

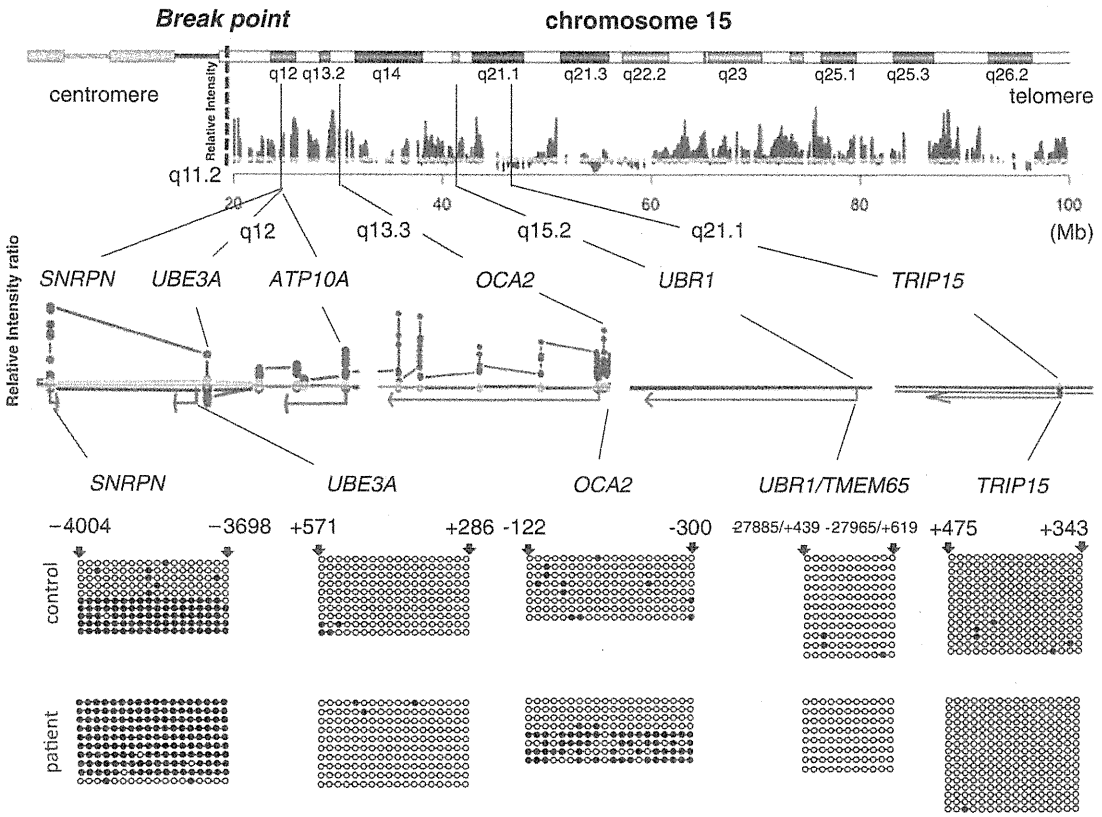

Fig. 4 DNA methylation analyses of CGIs in the chromosome 15 of the derivative X chromosome. *Upper panel*: profile of the DNA methylation difference between the chromosome 15 segment of the patient's derivative X chromosome and the chromosomes 15s of two healthy controls obtained by MeDIP analysis using CGI microarray analysis. *Middle panel*: enlarged view of the MeDIP analysis for genes on chromosome 15. *Spots* indicate the genomic positions of the oligonucleotides used for hybridization in the microarray assay, were designed within the CGIs of the genes. The *red arrows* indicate the transcriptional direction of the genes. The averages of hybridization determine the level of DNA methylation, which is shown as a *green* or *blue line*. *Lower panel*: bisulfite sequences of the CGIs on chromosome 15. *Open circle*: hypo-methylated CpG, *closed circle*: hypermethylated CpG. Genomic locations of the first and the last CpG in the sequence analyzed from the transcriptional start site are designated above the bisulfite sequence results

As expected, the CGIs of the genes in the distal region, *UBR1* and *TRIP15*, were not methylated (Fig. 4, middle and lower panels).

Distribution of transposable elements

We observed a high density of L1 elements in the upstream regions of the *SNRPN* and *OCA2* genes. However, the L1 density was low in the upstream region of the *UBE3A* gene. MIR elements were rarely detected in the upstream regions of all three genes. A high density of Alu transposable elements was observed in the upstream regions of the *SNRPN* gene, but not in the upstream regions of the *OCA2* and *UBE3A* genes.

Discussion

We molecularly characterized of the spread of XCI in an autosome of a boy with a t(X;15)(p21.1;q11.2) translocation. In this study, we found that (1) the *XIST* gene was active in the derivative X chromosome; (2) XCI and CGI hypermethylation constantly extended into the proximal region of the chromosome 15 section of the derivative X (breakpoint: ~15q14 [40 Mb from the centromere]); (3) CGI hypermethylation was not observed in the middle of 15q (15q21.1 [50 Mb]: q22.2 [60 Mb]); and (4) scattered CGI methylation was found in the distal 15q region (15q22.2 [60 Mb]: telomere). The CGI of *UBE3A* was not hypermethylated, although those of adjacent genes [e.g., the imprinted *SNRPN* gene and non-imprinted *ATP10A* (normally unmethylated)] (DuBose et al. 2010) were aberrantly hypermethylated. These results indicate that the spread of XCI from a translocated X chromosome is limited and gradually decreases (although it depends on the gene) in an autosome (Fig. 6).

As for the clinical relevance of these findings, the copy of Xq was completely inactivated in most of the cells, probably due to the selection of cells in which the derivative X

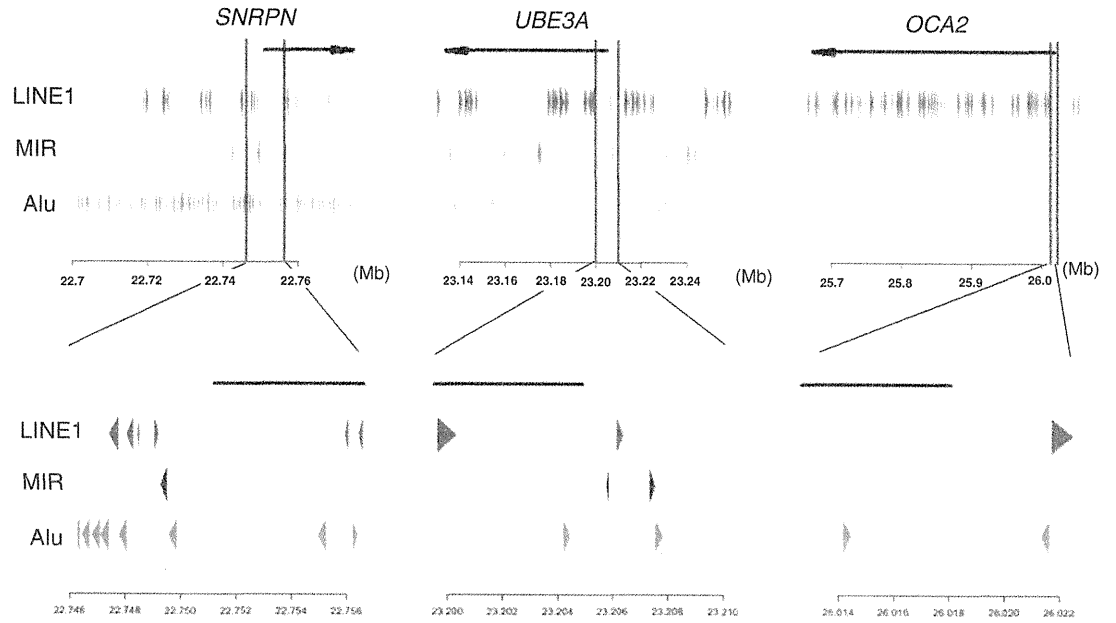

Fig. 5 Schematic illustration of the density of L1, MIR, and Alu repetitive sequences in the regions surrounding the transcription start sites of the *SNRPN*, *UBE3A*, and *OCA2* genes. A *triangle* (*red*, *black*, or *green*, respectively) indicates LINE1, MIR, or Alu sequences. The *direction* of each triangle indicates the transcriptional direction. The *SNRPN*, *UBE3A*, and *OCA2* gene regions are shown by the *arrows* at the *top*. The physical distance (Mb) from the telomere of the short arm of chromosome 15 is shown at the *bottom*

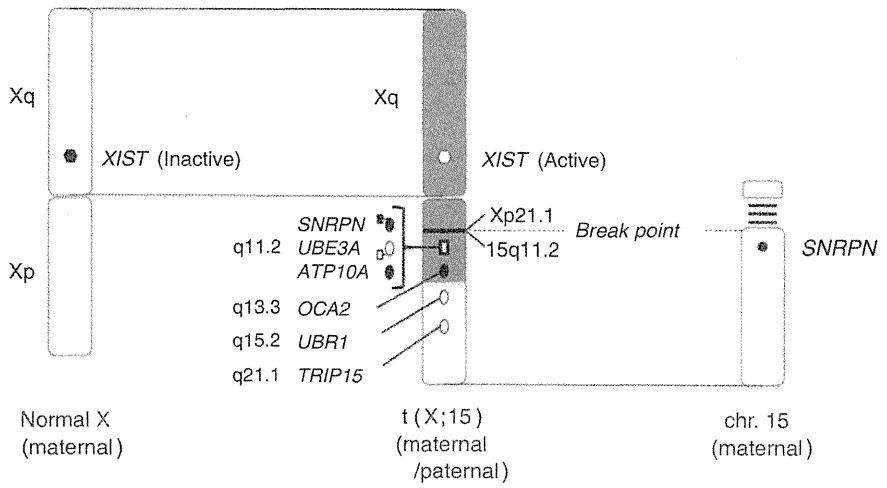

Fig. 6 Schematic representation of the molecular characterization of the patient with a t(X;15)(p21.1;q11.2) translocation. *Open circle* (*oval* and *hexagon*): hypo-methylated (active) gene, *closed circle* (*oval* and *hexagon*): hypermethylated (inactive) gene. *Open* and *closed squares* indicate low density and high density of LINE1 copies in the promoter regions of the genes, respectively

was active and the normal X was inactive during early development. Thus, some of the patient's clinical features should be due to gene inactivation caused by the spread of XCI, including *OCA2* and *SNRPN*, which may contribute to the hypo-pigmentation of the patient's skin and hair (Akahoshi et al. 2001; Brilliant et al. 1994) and the Prader–Willi syndrome-like features, respectively.

Wirth et al. reported a case with a translocation between chromosomes X and 15 [t(X;15)(q28;q12)]. In this case, the translocation was balanced (no monosomy), The XCI pattern was random (42:58), and XCI did not spread into the chromosome 15 part of the derivative X chromosome (Wirth et al. 2001). Because *SNRPN* and the adjacent *HBII-85* C/D box snoRNA (a transcript presumably related to the PWS phenotype) were disrupted by the breakpoint located in 15q12, the patient showed PWS-like features, such as obesity with an obsession for food, hypogonadism, and mental retardation at the age of 20 years, but did not have characteristic facial features, neonatal episodes of muscular hypotonia or failure to thrive. On the other hand, our patient's condition was more severe than the case of Wirth et al. and had features not described in that study, probably

because our patient not only had inactivation of the genes in the proximal chromosome 15 by XCI spread (including *SNRPN*) but also had a larger monosomic region of Xptel-p21.1, although the proportion of the cells, in which the der(X) was active, was small.

Several cases with XCI spread to the translocated autosome have been reported (Orellana et al. 2001; Sharp et al. 2001; Solari et al. 2001; Stankiewicz et al. 2006). Among these cases, the majority have shown the spread of XCI in an autosome (e.g., chromosomes 10, 14, and 15) (Orellana et al. 2001; Sharp et al. 2001; Stankiewicz et al. 2006). However, a few cases have not shown such a spread (e.g., chromosomes 2 and 21) (Solari et al. 2001). Thus, it may depend on the presence of certain features that facilitate XCI spread in the vicinity of the breakpoint on an autosome (Stankiewicz et al. 2006; Wirth et al. 2001). It has been suggested that XIST needs some sort of genomic "way station" to aid its spread, (Gartler and Riggs 1983) and that a certain class of transposons called long interspersed (LINE1 or L1) elements, (Lyon 1998) which are enriched on the X chromosome compared with autosomes, (Bailey et al. 2000; Popova et al. 2006) may be candidates for these way stations. It was recently discovered that LINE elements were expressed and their transcripts co-localize with the *XIst*-coated X chromosome during the X-inactivation time window in mice, LINE1 expression was observed in an autosome around an *Xist* gene that was integrated into a mouse autosome, and the efficiency of silencing by *Xist* correlates with the local concentration of full-length and truncated LINEs during the establishment and maintenance of inactivation (Chow et al. 2010). If these observations are true for each gene, then the "de novo" DNA methylation in the CGI of *SNRPN* and *OCA2* may represent the high silencing efficiency of *XIST* due to the high local concentration of LINE1, whereas the "escape from de novo DNA methylation" in the CGI of *UBE3A* may represent the low silencing efficiency of *XIST* due to the low local concentration of LINE1. Contrary to the situation with LINE1, Alu repetitive elements are thought to be more enriched in genes that escape inactivation (Wang et al. 2006) and, similar to LINE1, MIR elements are found at low levels in genes that escape inactivation (Ke and Collins 2003). However, our data did not support these hypotheses because *UBE3A* did not have a higher density of Alu repeats or a lower density of MIR elements than *SNRPN* in our study. Further extensive analysis at multiple distal genes will be necessary to elucidate the "way station" hypothesis in the spread of XCI in an autosome.

Since the HUMARA assay used in this study has an error rate <5% (Kubota et al. 1999), the patient's ratio (89:11) did not indicate a non-random (extremely skewed) XCI pattern. Thus, this result indicates the possible existence of a mosaic pattern and/or cells in which the derivative X is active. However, we did not find direct evidence for either of these possibilities, either by G-banding karyotyping (50 cells) or by replication R banding analysis (100 cells), respectively. If there are cells in which the derivative X is active and the normal X is inactive, then Xp (21.1-tel) monosomy can affect the phenotype; however, we did not observe the typical features described in females with Xp monosomy (Ogata et al. 1998), possibly because the proportion of these cells with an active derivative X and inactive normal X is low (~11%). It is also possible that some of the patient's features (e.g., cryptorchidism and hypogenitarism) may be caused by a Klinefelter-like karyotype, rather than inactivation of the PWS critical region on chromosome 15, since the patient had two X chromosomes and one Y chromosome (although one X chromosome is deleted between Xp21.1-p tel).

For the mechanism leading to the translocation, we can deduce that the initial event was a non-disjunction of the X chromosomes during maternal meiosis I, since the patient carried both maternal homologs. The translocation onto the X chromosome may be post-zygotic, given the juxtaposition of the paternal 15q on the maternal X chromosome. Furthermore, the absence of mosaicism, as determined from the cytogenetic (BrdU staining) and molecular (HUMARA assay) studies, imply the possibility that the translocation occurred very early during development, probably during the first post-zygotic divisions, as seen in a previous report (Orellana et al. 2001).

In summary, we demonstrated the extent and tendency of XCI spreading in an autosome in terms of DNA methylation using a microarray-based method. Further studies in different cases with t(X;A) translocations will contribute to a better understanding of the pathogenesis of congenital and acquired diseases, including hematological malignancies (Manola et al. 2007; Vassiliou et al. 2006) and may elucidate the properties of genes that determine whether they are subjected to or escape XCI.

Acknowledgments We thank the patient and their parents for their cooperation in this study and Professor Emeritus Tadashi Kajii for his critical reading of the manuscript. This research was supported in part by Grants-in-Aid for Scientific Research (S.S. and T.K.), Exploratory Research (T.K.) from the Ministry of Education, Culture Sports, Science, and Technology, Japan, and the Kawano foundation for medical research (T.K.), and Kawano Masanori Foundation for Promotion of Pediatrics (S.S.).

Conflict of interest None.

References

Akahoshi K, Fukai K, Kato A, Kimiya S, Kubota T, Spritz RA (2001) Duplication of 15q11.2-q14, including the P gene, in a woman with generalized skin hyperpigmentation. Am J Med Genet 104:299–302

Bailey JA, Carrel L, Chakravarti A, Eichler EE (2000) Molecular evidence for a relationship between LINE-1 elements and X chromosome inactivation: the Lyon repeat hypothesis. Proc Natl Acad Sci USA 97:6634–6639

Brilliant MH, King R, Francke U, Schuffenhauer S, Meitinger T, Gardner JM, Durham-Pierre D, Nakatsu Y (1994) The mouse pink-eyed dilution gene: association with hypopigmentation in Prader–Willi and Angelman syndromes and with human OCA2. Pigment Cell Res 7:398–402

Brown CJ, Ballabio A, Rupert JL, Lafreniere RG, Grompe M, Tonlorenzi R, Willard HF (1991) A gene from the region of the human X inactivation centre is expressed exclusively from the inactive X chromosome. Nature 349:38–44

Chow JC, Ciaudo C, Fazzari MJ, Mise N, Servant N, Glass JL, Attreed M, Avner P, Wutz A, Barillot E, Greally JM, Voinnet O, Heard E (2010) LINE-1 activity in facultative heterochromatin formation during X chromosome inactivation. Cell 141:956–969

DuBose AJ, Johnstone KA, Smith EY, Hallett RA, Resnick JL (2010) Atp10a, a gene adjacent to the PWS/AS gene cluster, is not imprinted in mouse and is insensitive to the PWS-IC. Neurogenetics 11:145–151

Gartler SM, Riggs AD (1983) Mammalian X-chromosome inactivation. Annu Rev Genet 17:155–190

Giorda R, Bonaglia MC, Milani G, Baroncini A, Spada F, Beri S, Menozzi G, Rusconi M, Zuffardi O (2008) Molecular and cytogenetic analysis of the spreading of X inactivation in a girl with microcephaly, mild dysmorphic features and t(X;5)(q22.1;q31.1). Eur J Hum Genet 16:897–905

Herzing LB, Romer JT, Horn JM, Ashworth A (1997) Xist has properties of the X-chromosome inactivation centre. Nature 386:272–275

Ke X, Collins A (2003) CpG islands in human X-inactivation. Ann Hum Genet 67:242–249

Kubota T, Nonoyama S, Tonoki H, Masuno M, Imaizumi K, Kojima M, Wakui K, Shimadzu M, Fukushima Y (1999) A new assay for the analysis of X-chromosome inactivation based on methylation-specific PCR. Hum Genet 104:49–55

Kubota T, Wakui K, Nakamura T, Ohashi H, Watanabe Y, Yoshino M, Kida T, Okamoto N, Matsumura M, Muroya K, Ogata T, Goto Y, Fukushima Y (2002) The proportion of cells with functional X disomy is associated with the severity of mental retardation in mosaic ring X Turner syndrome females. Cytogenet Genome Res 99:276–284

Lee JT, Jaenisch R (1997) Long-range cis effects of ectopic X-inactivation centres on a mouse autosome. Nature 386:275–279

Lee JT, Strauss WM, Dausman JA, Jaenisch R (1996) A 450 kb transgene displays properties of the mammalian X-inactivation center. Cell 86:83–94

Lyon MF (1961) Gene action in the X-chromosome of the mouse (*Mus musculus* L.). Nature 190:372–373

Lyon MF (1962) Sex chromatin and gene action in the mammalian X-chromosome. Am J Hum Genet 14:135–148

Lyon MF (1998) X-chromosome inactivation: a repeat hypothesis. Cytogenet Cell Genet 80:133–137

Manola KN, Stavropoulou C, Georgakakos VN, Zoi K, Fisfis M, Evmorfiadis I, Zoi C, Pantelias GE, Stefanoudaki K, Sambani C (2007) Switch in X-inactivation in a JAK2 V617F-negative case of polycythemia vera with two acquired X-autosome translocations. Leuk Res 31:1009–1014

Ogata T, Wakui K, Muroya K, Ohashi H, Matsuo N, Brown DM, Ishii T, Fukushima Y (1998) Microphthalmia with linear skin defects syndrome in a mosaic female infant with monosomy for the Xp22 region: molecular analysis of the Xp22 breakpoint and the X-inactivation pattern. Hum Genet 103:51–56

Orellana C, Martinez F, Badia L, Millan JM, Montero MR, Andres J, Prieto F (2001) Trisomy rescue by postzygotic unbalanced (X;14) translocation in a girl with dysmorphic features. Clin Genet 60:206–211

Popova BC, Tada T, Takagi N, Brockdorff N, Nesterova TB (2006) Attenuated spread of X-inactivation in an X;autosome translocation. Proc Natl Acad Sci USA 103:7706–7711

Schmidt M, Du Sart D (1992) Functional disomies of the X chromosome influence the cell selection and hence the X inactivation pattern in females with balanced X-autosome translocations: a review of 122 cases. Am J Med Genet 42:161–169

Sharp A, Robinson DO, Jacobs P (2001) Absence of correlation between late-replication and spreading of X inactivation in an X;autosome translocation. Hum Genet 109:295–302

Sharp AJ, Spotswood HT, Robinson DO, Turner BM, Jacobs PA (2002) Molecular and cytogenetic analysis of the spreading of X inactivation in X;autosome translocations. Hum Mol Genet 11:3145–3156

Sharp AJ, Migliavacca E, Dupre Y, Stathaki E, Sailani MR, Baumer A, Schinzel A, Mackay DJ, Robinson DO, Cobellis G, Cobellis L, Brunner HG, Steiner B, Antonarakis SE (2010) Methylation profiling in individuals with uniparental disomy identifies novel differentially methylated regions on chromosome 15. Genome Res 20:1271–1278

Solari AJ, Rahn IM, Ferreyra ME, Carballo MA (2001) The behavior of sex chromosomes in two human X-autosome translocations: failure of extensive X-inactivation spreading. Biocell 25:155–166

Stankiewicz P, Kuechler A, Eller CD, Sahoo T, Baldermann C, Lieser U, Hesse M, Glaser C, Hagemann M, Yatsenko SA, Liehr T, Horsthemke B, Claussen U, Marahrens Y, Lupski JR, Hansmann I (2006) Minimal phenotype in a girl with trisomy 15q due to t(X;15)(q22.3;q11.2) translocation. Am J Med Genet A 140:442–452

Takagi N, Abe K (1990) Detrimental effects of two active X chromosomes on early mouse development. Development 109:189–201

Uehara S, Hanew K, Harada N, Yamamori S, Nata M, Niikawa N, Okamura K (2001) Isochromosome consisting of terminal short arm and proximal long arm X in a girl with short stature. Am J Med Genet 99:196–199

Vassiliou GS, Campbell PJ, Li J, Roberts I, Swanton S, Huntly BJ, Fourouclas N, Baxter EJ, Munro LR, Culligan DA, Scott LM, Green AR (2006) An acquired translocation in JAK2 Val617Phe-negative essential thrombocythemia associated with autosomal spread of X-inactivation. Haematologica 91:1100–1104

Wang Z, Willard HF, Mukherjee S, Furey TS (2006) Evidence of influence of genomic DNA sequence on human X chromosome inactivation. PLoS Comput Biol 2:e113

White WM, Willard HF, Van Dyke DL, Wolff DJ (1998) The spreading of X inactivation into autosomal material of an x;autosome translocation: evidence for a difference between autosomal and X-chromosomal DNA. Am J Hum Genet 63:20–28

Wirth J, Back E, Huttenhofer A, Nothwang HG, Lich C, Gross S, Menzel C, Schinzel A, Kioschis P, Tommerup N, Ropers HH, Horsthemke B, Buiting K (2001) A translocation breakpoint cluster disrupts the newly defined 3′ end of the SNURF-SNRPN transcription unit on chromosome 15. Hum Mol Genet 10:201–210

Xue F, Tian XC, Du F, Kubota C, Taneja M, Dinnyes A, Dai Y, Levine H, Pereira LV, Yang X (2002) Aberrant patterns of X chromosome inactivation in bovine clones. Nat Genet 31:216–220

Yang X, Smith SL, Tian XC, Lewin HA, Renard JP, Wakayama T (2007) Nuclear reprogramming of cloned embryos and its implications for therapeutic cloning. Nat Genet 39:295–302